3-2021

Modeling Aircraft Disturbance Fields for Magnetic Navigation Using Dense ANNs and the Novel MANNTL Architecture

Kyle A. Emery

AFIT-ENG-MS-20-M-034

MODELLING AIRCRAFT DISTURBANCE FIELDS FOR MAGNETIC NAVIGATION USING DENSE ANNs AND THE NOVEL MANNTL ARCHITECTURE

THESIS

Presented to the Faculty

Department of Electrical and Computer Engineering

Graduate School of Engineering and Management

Air Force Institute of Technology

Air University

Air Education and Training Command

in Partial Fulfillment of the Requirements for the

Degree of Master of Science in Electrical Engineering

Kyle A Emery, B.S.E.E., B.S.E.E.

Second Lieutenant, USAF

March 19, 2020

AFIT-ENG-MS-20-M-034

MODELLING AIRCRAFT DISTURBANCE FIELDS FOR MAGNETIC NAVIGATION USING DENSE ANNs AND THE NOVEL MANNTL ARCHITECTURE

THESIS

Kyle A Emery, B.S.E.E., B.S.E.E.
Second Lieutenant, USAF

Committee Membership:

Joseph A Curro, Ph.D
Chair

Aaron J Canciani, Ph.D
Member

David Woodburn, Ph.D
Member

AFIT-ENG-MS-20-M-034

Abstract

The ability to use GPS for navigation is becoming increasingly limited in certain areas of the world. Knowing this, the Air Force Research Labs is constantly looking for ways to improve alternate navigation methods such as magnetic navigation. In the interest of making advancements in aircraft disturbance field modelling, Lieutenant Emery recreates models from previous works to prove results. Lieutenant Emery also introduces a novel model architecture that attempts to mix the filtering properties of Tolles-Lawson with the non-linear capabilities of an artificial neural network. The introduction of this model could present better aircraft disturbance field modelling and in turn, more reliable magnetic navigation in regions where GPS is not available.

Table of Contents

Page

List of Figures

List of Tables

MODELLING AIRCRAFT DISTURBANCE FIELDS FOR MAGNETIC NAVIGATION USING DENSE ANNs AND THE NOVEL MANNTL ARCHITECTURE

I. Introduction

1.1 Problem Background

The Global Positioning System (GPS) is always the preferred method of navigation because of it is accuracy and widespread applicability. However, GPS is very easy to jam by either spoofing or outright denial of service[9]. When GPS is lost, a pilot will still need to know where they are and the question becomes "What combination of alternate navigation methods are available?". There are a few methods of Alternate Navigation (AltNav) that can currently be considered by the pilot such as star tracking, terrain feature matching, and inertial navigation systems. All of these AltNav methods have the same benefit, they are still usable when GPS is jammed. However, AltNav methods have their own drawbacks as well - star tracking can only be used at night and when the sky above the aircraft is mostly clear[10]. Terrain matching only works when there are terrain features to match, trying to find differences, or features, in terrain over large bodies of water is impossible because the terrain is so similar in all directions[11]. Inertial navigation, while it can be very accurate initially, slowly becomes less accurate over time and is limited by the ability of the instrumentation onboard the aircraft[12]. Even with these drawbacks, these methods of AltNav can prove to be very helpful when they are available and when they are also able to work together in the platforms navigation system. In that light, adding another method of

AltNav to the repertoire would make for a more robust system that can make more accurate absolute position estimates and, at the same time, constrain estimate errors over longer periods of time.

1.1.1 Magnetic Navigation

Magnetic navigation is currently a growing field of interest not only for military application but for civilian use as well. The allure of a practically unjammable, ever-present form of alternate navigation is the cause for such growth and research[2]. The limitations of practical Magnetic Navigation (MagNav) use are still large problems to solve though. The lack of consistent, accurate, and modern magnetic maps is one such limitation. However in Canciani's 2016 paper he alleviated some of these concerns about the feasibility of MagNav. To start, Canciani showed the slow rate at which magnetic maps diverge over time[2]. While comparing two highly accurate magnetic maps taken over the same area, 3 years apart, and while factoring in temporal and Tolles-Lawson connections he demonstrated a disagreement standard deviation of only 1.55nT between the two maps. This finding alone does well to prove the sustainability of MagNav for AltNav. Next, in a flight experiment conducted for his paper, designed as a proof of concept, Canciani was able to navigate within a pre-mapped route and showed a Distance Root Mean Square (DRMS) error of only 13.1 m over the course of a single 1-hour flight. During the same flight the accuracy of an unaided inertial navigation sensor (INS) aboard the aircraft had strayed to 344 m DRMS[2].

In a second flight experiment conducted for Canciani's paper, a new map and navigation set up was used for a long-distance, cross-country flight. For this second flight, the North American Magnetic Anomaly Database (NAMAD) map was utilized. The NAMAD map is a patchwork database of magnetic data encompassing the North American continent and collected over time and with multiple flights. Admit-

tedly, the quality of the NAMAD map is much lower than the survey map used in Canciani's proof of concept flight experiment. This is largely attributed to the uncertainty in whether or not the GPS capabilities of the aircraft collecting NAMAD data were highly accurate. Using this map strictly for MagNav was not the point of the experiment though. MagNav in this flight was used to help constrain the deviation of the onboard INS. The results showed that an unaided tactical INS drifted nearly 50 km over the 5-hour cross-country flight. But, when aided by MagNav, this error was constrained to only 3 km, a massive improvement. With the same data used, in order to demonstrate how vital a good quality map is to navigation, Canciani simulated a map of the same quality depicted in the first flight. After simulating this map the same experiment was performed. An unaided INS was able to navigate within 1.5 km where the INS and MagNav coupling could achieve 600 m accuracy for the same 5-hour flight.

1.2 Research Objectives

Continuing on initial proof of concept provided in Hezel's thesis, machine learning algorithms will be compared to the abilities of Tolles-Lawson (TL) and Augmented Tolles-Lawson (ATL)[13]. The work performed in the 2020 paper showed that machine learning's ability to model the aircraft disturbance was much better than both TL and ATL on a small wooden Unmanned Aerial Vehicle (UAV) modded with magnets on the control surfaces. While this showed that machine learning could predict the aircraft disturbance field with incredible accuracy compared to TL, the aircraft used to test this was very simple compared to the aircraft that these algorithms and models would actually be used on. The main goal for this thesis is to test how accurately machine learning can model and predict aircraft disturbance field on a more realistic and more complex aircraft - in this case, an F-16. A second goal is to try a new

algorithm that mixes the strengths of Tolles-Lawsons filtering capabilities and the non-linear function mapping ability of an Artificial Neural Network (ANN).

1.3 Document Overview

Chapter II, explains the concepts behind magnetic navigation and aircraft disturbance field modeling. Concepts like anomaly fields, the origin of the aircraft disturbance field, and current methods of removing the aircraft disturbance field from magnetometer measurements. Chapter III details the data used in this thesis, experiments performed on the data and the novel MANNTL model. Chapter IV presents the results from experiments detailed in chapter III and explores the significance of the results. The final chapter, chapter V, reviews the findings from the experiments in chapter IV and offers possible future improvements to attempted methods of modeling the aircraft disturbance field.

II. Background and Literature Review

2.1 Chapter Overview

Chapter II will cover topics important to the experiments that will be performed for this thesis. The onboard scalar and vector magnetometers will pick up magnetic signals from many different sources. The magnetometers alone cannot differentiate between the sources and therefore, knowledge about the signals it is picking up must be covered in hopes of being able to either isolate desired signals or remove unwanted ones. A few of Earth's total magnetic field components, described in 2.2, are not helpful and need to be compensated for in order to isolate the crustal anomaly field. There are many necessary steps in order for proper aircraft calibration to be performed.

Methods to remove the measured aircraft field will be covered in this chapter as well such as Tolles-Lawson (TL) and its augmented form, Augmented Tolles-Lawson (ATL), covered in sections 2.4 and 2.5. These algorithms as well as accompanying flight patterns, described in Section 2.4.1, can aid in isolating the aircraft disturbance field.

Aside from TL and ATL, there are proposed newer methods of dealing with aircraft disturbance fields such as utilizing machine learning and neural networks. More information on neural networks can be found in Section 2.6. Machine learning has the potential to model the aircraft disturbance field with or without the necessary filtering step found in TL and ATL.

2.2 Earth's Total Magnetic Field

There are multiple sources that contribute to Earth's total magnetic field. Earth's core field, crustal field, and ionospheric/space weather effects. Of these three, the most powerful by far is Earth's core field. The core field is generated within the

Earth's core where the magnetic signal is intense and unpredictable. However, the further away a magnetic source is measured, the more it begins to look like a uniform magnetic dipole. This effect can be seen in Fig. 1

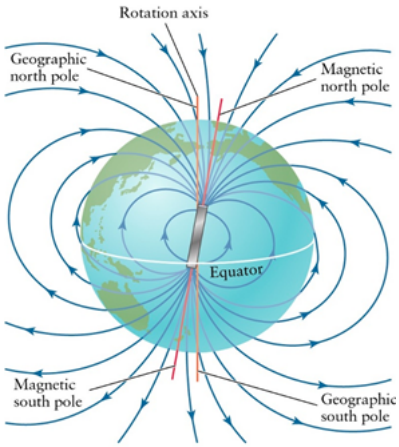

Figure 1: Earth's core field[1]

At the surface of the earth, the dipole effect has nearly completely taken over and the Earth's core field is mostly uniform around the globe much like the magnetic field given off by a common bar magnet. That is not to say its intensity doesn't change around the globe though, the intensity of Earth's core field can vary between 23,000nT and 67,000nT depending on location and altitude[14]. Were this the only magnetic field within Earth's structure, only heading would be able to be determined when navigating, such as with a compass. Magnetic Navigation (MagNav) is concerned with absolute positioning though and will require more details from the surrounding magnetic field. Within Earth's crust there are numerous, albeit less powerful, magnetic sources that can be used in this regard.

2.2.1 Crustal Field

The second major piece of Earth's magnetic field to be considered in measurements is the crustal field. The crustal field is generated by large deposits of material

within the lithosphere that either naturally generate their own magnetic field, such as magnetite, or ferrous materials that have a magnetic field because they lay within, and are influenced by, Earth's core magnetic field. The crustal field is generated by large deposits of either permanently magnetic material or ferromagnetic materials. Permanent magnets generate their own naturally occurring magnetic field and can add or detract from any surrounding magnetic fields. Unlike permanent magnets, ferromagnetic materials generate a magnetic field only while lying within another magnetic field. In the case of materials within the crustal field, this is often Earth's core field or even the magnetic field of a neighboring permanent magnet or similarly ferromagnetic material.

The intensity of the crustal field ranges on the scale of hundreds of ηT as compared to the core fields tens of thousands nT scale mentioned previously[14]. Although the scale of the crustal field pales in comparison the core field, the spacial frequency of the crustal field is much higher. The variation that the crustal field provides for interesting "landmarks" on magnetic survey maps which will be the main driver for absolute position and navigation. Since the crustal field is ultimately what is used to navigate, it makes sense to try to isolate it from the other magnetic signals i.e. the Earth core field. The intensity of a crustal source can be determined by comparing the measured field at any given point on the Earth, to a reference of Earth's core field at the same point. A reference field, such as the commonly used International Geomagnetic Reference Field (IGRF), provides a standard world-wide Earth core field model with which to do this.

Fig. 2 shows how the anomaly component, $B_{anomaly}$, can be derived from the measured field, B_{total}, and the reference field, B_{core}.

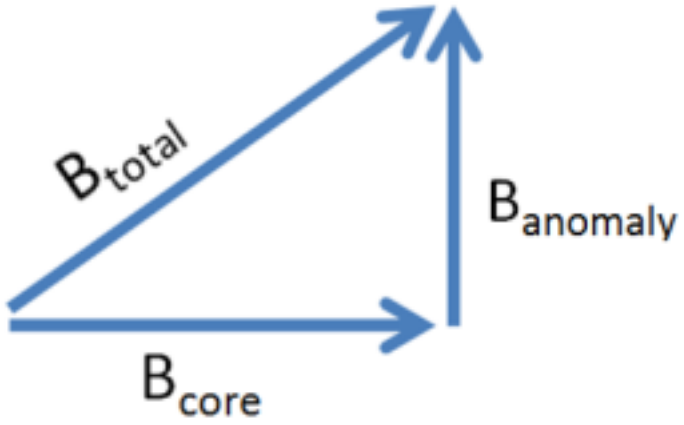

Figure 2: Anomaly from perpendicular crustal and core field measurement[2].

2.2.2 Ionospheric Effects - Solar Quiet currents (SQs)

The final piece to be discussed in magnetic survey readings originating from points exterior to an aircraft are ionospheric effects. Throughout the course of a day, sunlight bombards the ionosphere and ionizes air molecules. This ionization creates a slight variation in ambient magnetic intensity, deemed SQs currents, and can be detected by stationary base stations equipped with sensitive magnetometers that constantly collect magnetic data through the day such as in Figures 3 and 4. The SQ data collected by a base station, since this effect has a wide reaching effect and would be common between the base station and magnetometer, can then easily be subtracted from the measurements of a magnetometer.

The scale of these SQ readings generally take place on the scale of tens of nT. Although this fluctuation is not large relative to crustal and Earth fields, it can still throw off navigation if not taken into account. This is why a reference to a nearby base station is recommended, should it exist.

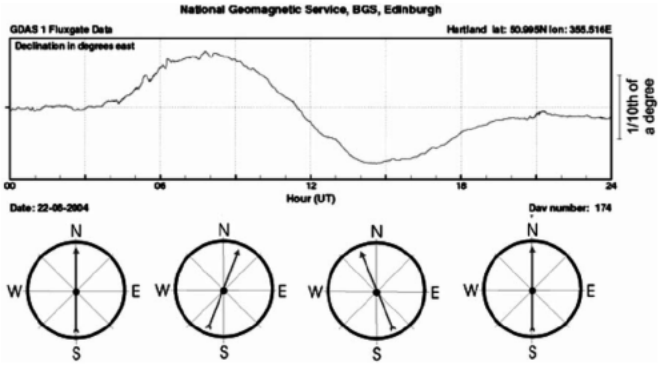

Figure 3: Exaggerated compass declination effects due to SQ currents[3].

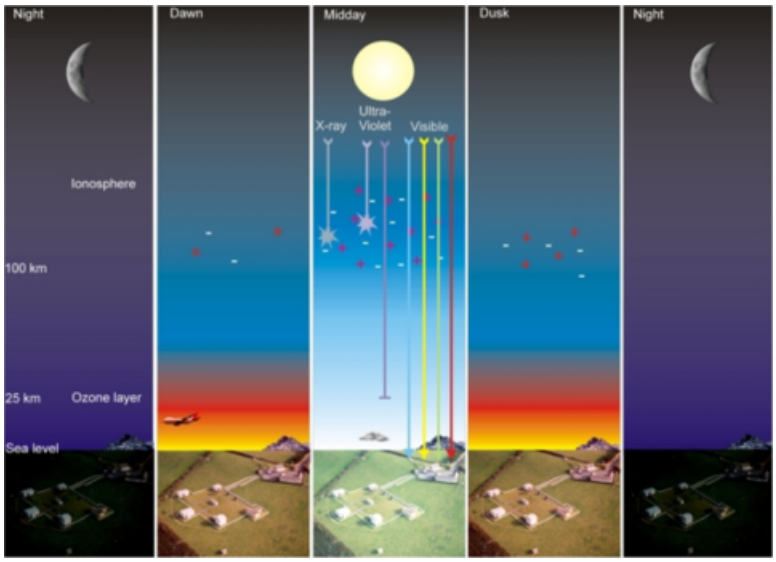

Figure 4: Ionization of atmosphere creating SQs[3].

2.3 Collecting and Managing Data

2.3.1 Aircraft Magnetic Field

The previous section explored the biggest considerations when measuring Earth's total field but Earth's total field is not all that a magnetometer will measure. There are many man-made contributions to the measured magnetic intensity. Man-made interference is common around metallic objects like airplanes, power lines, and buildings. Thus, to get readings of the crustal field the man-made interference must be removed. Moving further from power lines and buildings is a simple way to remove such interference when calibrating an aircraft. The aircraft has the potential to be a huge source of magnetic signal which, for aircraft calibration purposes, the goal is to accurately model the aircraft noise and remove it. An aircraft and its subsequent subsystems are composed of components that can be magnetically inert, permanently magnetized, ferromagnetic, or can create their own magnetic field when electrical current is run through them. For example, should a magnetometer be placed near the engine block of an aircraft, there are many moving metal pieces coupled with high current components that, added up, make for a particularly violent magnetic environment that can vary on the scale of thousands of nT as can be seen in Figure 5.

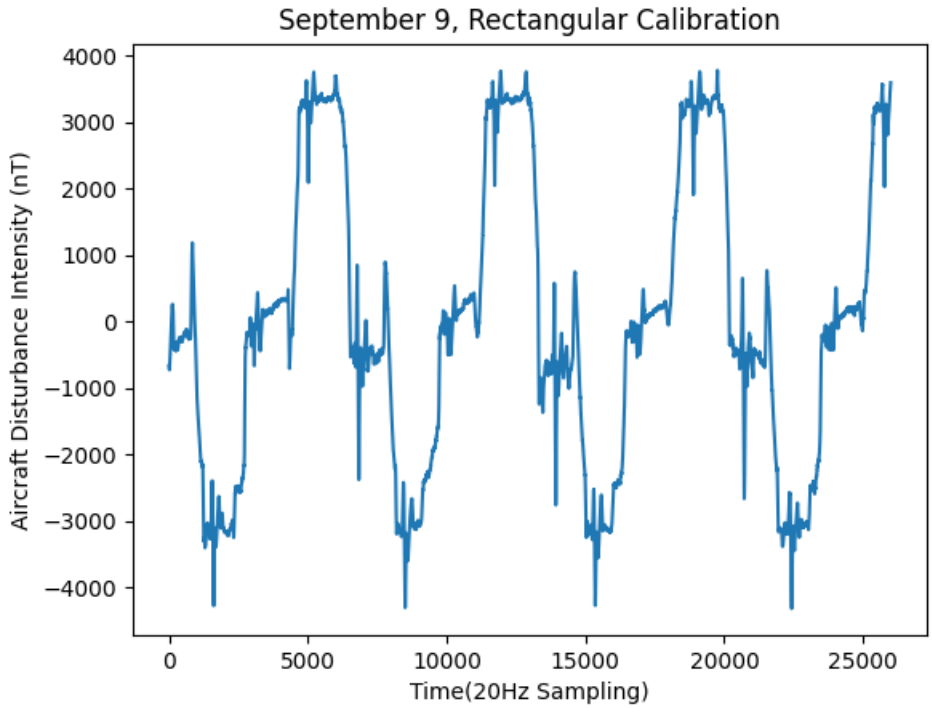

Figure 5: Scale of the Aircraft Disturbance Field while flying a rectangular pattern

This scale is roughly the same scale as Earth's crustal field discussed in section 2.2.1. If a magnetometer were to be placed in an engine block, as in the previous example, surveying and navigation would be impossible using the current calibration techniques such as TL or ATL. If highly accurate surveying and navigation is to be achieved, the location of the magnetometer on or within an aircraft is an important factor. Before detailing common placement of magnetometers for surveying, it is important to mention that magnetic signals decay at a rate of $1/r^3$, r being the radius from any relevant magnetic source[15]. Given this rate of decay, in order to minimize aircraft noise, surveyors place a magnetometer as far from the aircraft interference as possible; typically on a boom, or stinger, that extends out the rear of the aircraft. Another method of minimizing aircraft noise is to place the magnetometer on a sling that hangs below the aircraft[16]. Both of these methods are effective at minimizing noise due to the rate of decay magnetic signals are subject to. While both methods

minimize noise, they often do not completely remove the aircraft noise. However, with the help of a calibration method known as TL, detailed in a following section, aircraft noise can be further removed from measurements resulting in highly accurate survey maps. These survey maps will be heavily utilized in the coming experiments.

2.3.2 Survey Maps

Accurate aerial magnetic survey maps can be created with a specialized survey aircraft. With these specialized aircraft, the aircraft disturbance field can be effectively removed from measurements with well known calibration methods. However, when the magnetometer is placed inside the aircraft, survey maps are essential and must already be present to serve as truth data. In navigation these maps will serve as reference to the pilot to determine absolute positioning. Understanding how they're created will be useful in the coming calculations and when trying to create truth data.

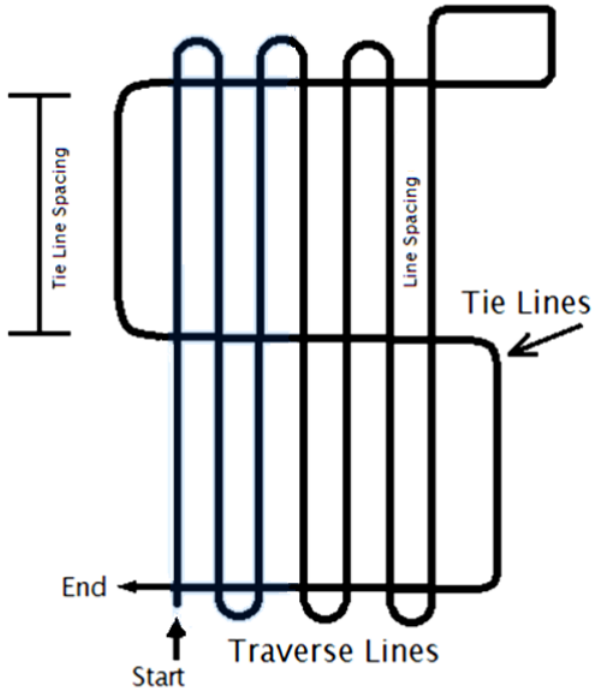

Figure 6: Pattern for magnetically surveying an area

Collecting survey data is done in a methodical manner in order to reduce the amount of flight time required and still achieve maps without loss of information. First, as mentioned before, a magnetometer is placed on a boom to ensure the cleanest readings possible. Next, an altitude must be chosen to take the measurements. The chosen survey altitude must be far enough above any man-made interference, such as buildings, but not so high that crustal field anomalies can't be measured. Now that an altitude is selected, a sufficient spacing interval for the planned route is the next step. Since the Earth's core field and crustal field decay at a rate of $1/r^3$, the higher the altitude, the more the main dipole effect dominates the signal. For example, if a survey aircraft were to fly at 1000 m above ground and record a magnetic map then fly the same route but at 2000 m the second map would overall have the same large features but would be much smoother as seen in Fig. 7. The Earth's crustal field is made up of many smaller, higher spacial frequency fields. This higher spacial frequency, decaying at $1/r^3$, creates higher magnitude spikes at lower altitudes that smooth over as they are observed at further distances from the source.

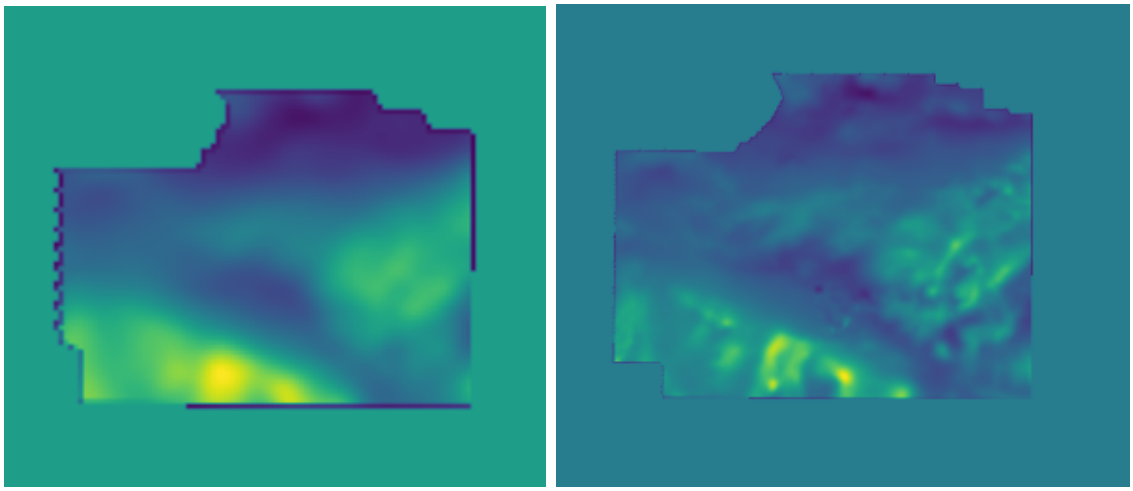

Figure 7: Aerial Magnetic Survey Maps Provided for Edwards AFB, California. Left: 5,486 m altitude survey. Right: 1200 m altitude survey. Notice the difference in definition between the two maps caused by the altitudes at which they were collected.

This can be likened to how a low pass filter would act upon a signal. Taking this into account, the spacing in which a map should be surveyed should be no more than a quarter of the altitude at which the aircraft is flying in order to fully sample the map[17]. For example, if a map is surveyed at 1200 m altitude the spacing for data collection should be no more than 300 m wide. This altitude to spacing ratio ensures adequate magnetic field coverage so as not to miss out on any important information.

2.3.3 Interval Continuation

While magnetic maps must be present in order to perform navigation, it is not feasible to try to survey at all possible altitudes that an aircraft might fly. Fortunately, once an area of Earth's magnetic field is surveyed, it is not hard to calculate the intensity of Earth's field above the measured altitude. There are two ways to do this, upward continuation and interval continuation[18].

Upward continuation requires only one available survey map of an area below the pilots current altitude. Upward continuation can work very well if the pilot is flying just above the plane in which magnetic map was collected. Much like how the base of a pyramid grows larger as the pyramid gets taller with a fixed slope on its sides. The higher above the map the pilot is, the larger the survey map beneath them must be in order for upward continuation to remain effective. At continually higher altitudes, upward continuation operates on the assumption that the pilot has an infinitely large survey map beneath them.

Interval continuation requires two prerecorded magnetic survey maps. One map, or tile, being at a lower altitude, a_0, and another tile at a higher altitude, a_h, as shown in Equation 1. Overall, interval continuation is much more reliable when between the two provided maps than upward continuation with only one map. This is because of the assumption stated before about upward continuation. Upward continuation needs

larger maps at higher altitudes in order to be accurate. Whereas interval continuation, as long as there is a map above and below the current altitude, is like connecting to dots between the two map planes. To perform interval continuation, the following equations are used[18].

$$F(M_z) = \frac{1}{q} \begin{bmatrix} e^{+(z-H)k} - e^{-(z-H)k} \\ e^{-zk} - e^{+zk} \end{bmatrix}^T \begin{bmatrix} F(M_0) \\ F(M_h) \end{bmatrix} \tag{1}$$

$$q = e^{-Hk} - e^{+Hk} \tag{2}$$

where:

- z is the altitude above the lower tile
- $F(M_z)$ is the Fourier Transform of the desired tile at altitude z
- $F(M_0)$ is the Fourier Transform of the lower tile
- H is the height between the upper and lower tiles
- $F(M_0)$ is the Fourier Transform of the upper tile
- k is equal to the grid wavenumber, $|k| = \sqrt{k_x^2 + k_y^2}$
- k refers to the absolute value of the wavenumber in the frequency domain.

Using the interval continuation equations along with the two prerecorded maps returns a whole third map, $F(M_z)$, that will inverse Fourier transform will need to be performed on. This generated map is an exact representation of the magnetic intensity found at that altitude z.

2.4 Tolles-Lawson Algorithm

As mentioned in the previous section, when aerial magnetometer data is collected, there are two major sources to be considered - the Earth total field and aircraft disturbance field. The total measured magnetic intensity can be represented as:

$$B_{(measured)} \approx B_{(Earth)} + B_{(aircraftdist)} \tag{3}$$

where:

$$B_{(Earth)} = B_{(core)} + B_{(crustal)} + B_{(SQ)} \tag{4}$$

The TL algorithm is the traditional way of removing an aircraft's magnetic noise from magnetometer measurements. TL works under a few assumptions to keep in mind - first, is that the relationship of $B_{aircraft}$ to B_{Earth} is such that:

$$|B_{aircraft}|^2 \gg |B_{earth}|^2 \tag{5}$$

Implying that $B_{aircraft}$ is much smaller than B_{earth}. From section 2.3.1, we know this is not true but TL can still operate, albeit with less effectiveness, under these circumstances.

Assumption two is that $B_{total} \approx B_{earth}$, and the third assumption is that the only terms to be accounted for with respect to the aircraft are the permanent, induced, and eddy fields as shown in equation 6. With TL equations, these components can be modeled as[19]:

$$B_{(aircraft)} = B_{(permanent)} + B_{(induced)} + B_{(eddy)} \tag{6}$$

$$B_{(permanent)} = a_1 \cos\theta + a_2 \cos\phi + a_3 \cos\psi \tag{7}$$

$$\begin{aligned} B_{(induced)} = & B_t(a_4 cos^2\theta + a_5 cos\theta cos\phi + a_6 cos\theta cos\psi \\ & + a_7 cos^2\phi + a_8 cos\phi cos\psi + a_9 cos^2\phi) \end{aligned} \tag{8}$$

$$\begin{aligned} B_{(eddy)} = & B_t(a_{10} cos\theta (cos\theta)' + a_{11} cos\theta (cos\phi)' + a_{12} cos\theta (cos\psi)' \\ & + a_{13} cos\phi (cos\theta)' + a_{14} cos\phi (cos\phi)' + a_{15} cos\phi (cos\psi)' \\ & + a_{16} cos\psi (cos\theta)' + a_{17} cos\psi (cos\phi)' + a_{18} cos\psi (cos\psi)' \end{aligned} \tag{9}$$

The permanent field is created by magnetic elements within the aircraft itself. These elements generate their own constant magnetic field that is not influenced by the Earth's magnetic field moving around them. This differs from the other two types of aircraft magnetic noise accounted for in the TL algorithm. The first of which is the aircraft induced magnetic field is created by ferromagnetic chunks of materials in the aircraft. Ferromagnetic materials within an aircraft add constructively or deconstructively to an external magnetic field. They are also constantly changed with respect to the orientation of the aircraft within the external magnetic field - in this case, Earth's total field. Eddy currents are influenced by the change in an external magnetic field around the aircraft as well. However, they differ from the induced field in that Eddy currents occur within closed loop electrical systems where current can flow[17]. The rate of change in an external field drives further generation of magnetic fields within these circuits and hence needs to be represented by Tolles-Lawson.

Once permanent fields, induced fields, and eddy currents are calculated, these values will then be placed in an $S \times 18$ matrix, $\mathbf{A}$, such as in equation 10 where S is

the number of samples in the data set.

$$\mathbf{A} = \begin{bmatrix} Permanent & Induced & Eddy \\ (S \times 3) & (S \times 6) & (S \times 9) \\ \vdots & \vdots & \vdots \end{bmatrix} \tag{10}$$

The direction cosine terms from equations 7, 8, and 9 are calculated with the 3-axis fluxgate magnetometer, colocated with the much more accurate scalar magnetometer by:

$$\cos\theta = \frac{F_x}{B_t} \tag{11}$$

$$\cos\phi = \frac{F_y}{B_t} \tag{12}$$

$$\cos\psi = \frac{F_z}{B_t} \tag{13}$$

$$\text{where,} B_t = \frac{1}{S}\sum\sqrt{F_x^2 + F_y^2 + F_z^2} \tag{14}$$

F_x, F_y, and F_z are the fluxgate magnetometer measurements along the x, y, and z axes of the sensor.

The a coefficients displayed in equations 7, 8, and 9 are the TL coefficients that will be solved for using ordinary least squares regression. However, performing ordinary least squares regression on the **A** matrix in its current state would not be beneficial. The **A** matrix still contains information about the Earth total field as well as the aircraft disturbance field. Right now, it would be impossible to predict the aircraft disturbance field since it is not isolated. This is where the real magic of TL, the

bandpass filtering (bpf) applied to the A matrix from equation 10, takes place[19].

$$\begin{aligned} y_{(measured)} &= Ax \\ y_{(aircraft)} + y_{(earth)} &= Ax \\ \texttt{bpf}(y_{(aircraft)} + y_{(earth)}) &= \texttt{bpf}(Ax) \end{aligned} \tag{15}$$

Taking advantage of the fact that a bandpass filter is a linear operation, we can distribute it over addition. This bandpass filter has two effects. First, due to the relatively low spacial frequency of Earth's total magnetic field, it will be completely removed from the measurements after bandpass filtering at a high enough selected frequency band. Earth's total field is only present at a very low frequencies compared to the aircraft disturbance field. Second, the aircraft field will be severely reduced as well but due to the calibration pattern, detailed later in section 2.4.1, there will still be a small amount of aircraft signal to fit to. This reduction of signal is significant because while all measured magnetic signals are reduced, the aircraft signal is much more prominent in the filtered scalar measurements than the Earth field. The **A** matrix is similarly effected. After bandpassing, **A** is now left to represent the same small portion of aircraft signal that $bpf(y_{(aircraft)})$ does. Important to note, **x** is unaffected since it is a vector matrix of constants with no sense of time. **x** only represents the coefficients of the traditional Tolles-Lawson fit. The filtered aircraft

data is only useful for generating the coefficients found in $\mathbf{x}$.

$$\begin{aligned}
\texttt{bpf}(y_{(aircraft)} + y_{(earth)}) &= \texttt{bpf}(Ax) \\
\texttt{bpf}(y_{(aircraft)}) + \texttt{bpf}(y_{(earth)}) &= \texttt{bpf}(A)x \\
\texttt{bpf}(y_{(earth)}) &\cong 0 \\
\therefore \texttt{bpf}(y_{(aircraft)}) &\cong \texttt{bpf}(A)x
\end{aligned}$$

Since the coefficients of $\mathbf{x}$ were unaffected by the bandpass filter, they can be used to estimate the unfiltered aircraft signal.

$$y_{(aircraft)} \cong Ax$$

2.4.1 Calibration Flights

Calibration flights serve to help capture the aircraft disturbance signal within the desired frequency band mentioned in the previous section. There are two different calibration flights that can performed for this effect. The first being the high-and-tight, or rectangular, calibration and the second being the cloverleaf calibration. The calibration flights performed with the F-16 were done with a 60 Hz bandpass frequency in mind. The frequency 60 Hz will be used to help explain the concepts going forward although 60 Hz is not a strict frequency for these maneuvers. To clarify, the oscillations in yaw, pitch, and roll are not done at 60 Hz. The bandpass filter will filter around 60 Hz.

2.4.1.1 Rectangular Calibration

The rectangular pattern attempts to capture all of the aircraft noise within a narrow frequency band that complements the designed frequency band of the bandpass filter at 60Hz. The rectangular flight pattern has distinct characteristics that can be easily seen in Figures 8 and 9. As for why the flights are at a high altitude and tight working area has to do with minimizing any magnetic signal that is not the aircraft disturbance field. The high altitude contributes to the dipole effect from Section 2.2 while the small area reduces as much variation in external magnetic signal as possible.

The rectangular calibration pattern can be dissected into two different pieces. First is the 60Hz oscillations in all three axes(yaw, pitch, and roll), as can be seen in figure 9. Second, these three axes oscillations will be performed on all four headings of the rectangular pattern(SW, NW, SE, NE) as shown in figure 8.

2.4.1.2 Cloverleaf Calibration

The cloverleaf calibration flight operates on the same principal as the rectangular pattern. High altitude, small patterns, roll, pitch, and yaw maneuvers are all still a requirement. The difference is how the pattern is flown. The calibration pattern can be seen below in Figure 10.

Both of these flight patterns help to describe the aircraft noise as fully as possible within the assumptions of Tolles-Lawson. Due to the inevitable breaking of these assumptions, there are bound to be errors in the fit that can't be accounted for even in the simplest of aircraft. All in all, this is the traditional form of TL but more utility can be squeezed out of the TL algorithm if more information about the aircraft is available.

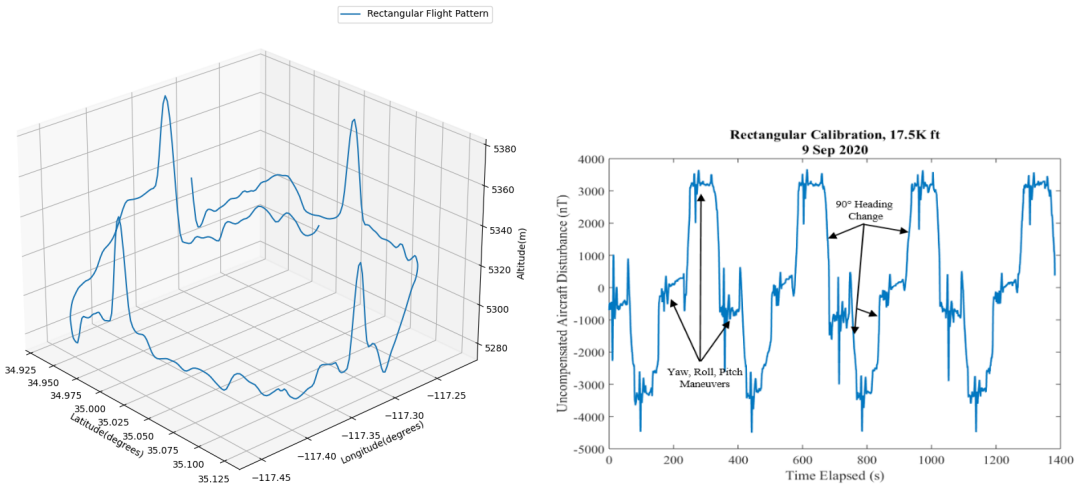

Figure 8: Left: 3D line plot of rectangular calibration pattern. Right: Scalar magnetometer measurements of rectangular calibration pattern

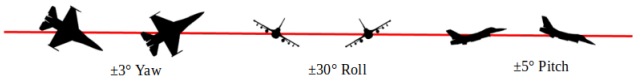

Figure 9: Visual description of yaw, roll, pitch maneuvers performed on each leg of rectangular pattern

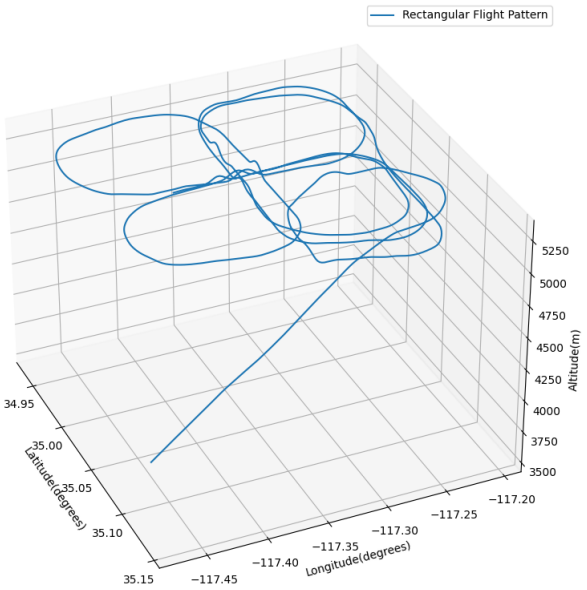

Figure 10: 3D line plot of cloverleaf flight pattern

2.5 Augmented Tolles Lawson

ATL is a means to extend the utility of traditional Tolles-Lawson. The Augmented Tolles-Lawson algorithm requires all of the same components - the 18 Tolles-Lawson coefficients, the calibration flight data, the band pass filter, and ordinary least squares regression to fit the unfiltered data[13]. ATL has an extra requirement though, a collection of supplementary data available to the aircraft that is meant to extend the third assumption of TL[13]. This supplementary data can be time data, instrument data, voltage and amperage usage for components and subsystems, whether an aircraft subsystem is on or off, the speed of a rotating subsystem etc. This collection of data will aptly be *augmented* onto the **A** matrix found with TL. Where S is the number of samples and N represents the number of augmentations added to Tolles-Lawson. See equation 16[13].

$$\mathbf{A} = \begin{bmatrix} Permanent & Induced & Eddy & Augmentations \\ (Sx3) & (Sx6) & (Sx9) & (SxN) \\ \vdots & \vdots & \vdots & \vdots \end{bmatrix} \tag{16}$$

By augmenting the data into the **A** matrix, a more well rounded view of the aircraft noise present in measurements can be seen since the third assumption of TL only takes into account permanent, induced, and eddy fields. However, not all data is helpful in this case. Some data may either be benign to the algorithm or detrimental and make it harder for the least squares regression to fit the data. Whether the data is helpful, benign, or detrimental is heavily dependent on where the magnetometers are placed within the aircraft. The closer the magnetometer is to a given source, the more it will help describe the overall measured aircraft noise.

Both TL and ATL, can be effective in their own right but both limited by the TL

assumptions listed in Section 2.4. These assumptions can be forgone by using machine learning which can create more complex functions with it is non-linear capabilities.

2.6 Machine Learning and Neural Networks

Machine learning and neural networks are growing research tools that allow for effective, complex functions to be created that map any given input to an output[7]. Today, machine learning and neural network models can be found in use every day in common applications like email filtering in your inbox, text prediction on your phones keyboard, and facial recognition in social media apps. These models can be created with a few different methods such as supervised learning, unsupervised learning, and reinforcement learning[20]. Supervised learning requires a set of input data, $\mathbf{X}$, as well a set of outputs, $\mathbf{Y}$, that stand as truth data in which the model should try to fit to. With $\mathbf{X}$ and $\mathbf{Y}$ available for supervised machine learning, the computer will make an attempt to generate a function, or model, that can be represented as $f(\mathbf{X}) = \hat{\mathbf{Y}} \approx \mathbf{Y}$. Unsupervised learning still requires an input the same as supervised learning but has a different goal - which is for the model to create relationships between the data on its own and/or find hidden relationships in data that may not be seen otherwise. Reinforcement Learning (RL) gives "rewards" to the neural network in the form of higher weights when desired "winning" conditions are met. For example, the winning conditions for chess are well defined - lock the opposing players king into a position where the other player has no moves left to prevent the checkmate. In chess though, there are a near infinite number of moves that could be made by either player over the course of a game. The sheer number of moves that could be made would make it an impossible problem to try to train a neural network through supervised learning where the desired output is known for every situation. The goal of RL is for the model to makes its own moves and decide whether or not certain behaviors were beneficial

to reaching the win condition - even if it does not win the game overall.

2.6.1 Learning Process

When training a model, whether with supervised, unsupervised, or reinforcement learning, there is a common process between them all in which a model is trained.

Figure 11 shows a common build for a neural network. A machine learning network is built with an input layer and an output layer. This is different from a neural network, which contains hidden layers. These hidden layers "deepen" the network and are the reason that neural networks are referred to as Deep Learning (DL) networks. All of the layers in a network contain neurons, shown by the circles in Figure 11. In each neuron, a number of operations take place. The input to each neuron is first multiplied by the weights corresponding to each input. The higher the weight applied to an input the more significant it is to the neuron. The resulting vector matrix is then summed into a scalar value and, if applicable, bias is added. The last step to take place within a neuron is to push this value through an activation function[5]. This process can be seen in Figure 12

Activation functions are responsible for the neural networks ability to form complex relationships in its model[6]. Four activation functions can be seen in Figure 13. Should the user elect to use only the linear activation function in their model, the model would be simplified to something resembling a multivariate linear regression. However, there are typically a multitude of non-linear activation functions such as the Rectified Linear Unit (ReLU), Sigmoid, and Hyperbolic Tangent (TanH) as shown in Figure 13.

Once the all neurons in a given layer have completed this mathematical process the calculated outputs are then passed to the next layer. This is referred to as forward-propagation. Forward-propagation repeats for each layer until the model reaches the

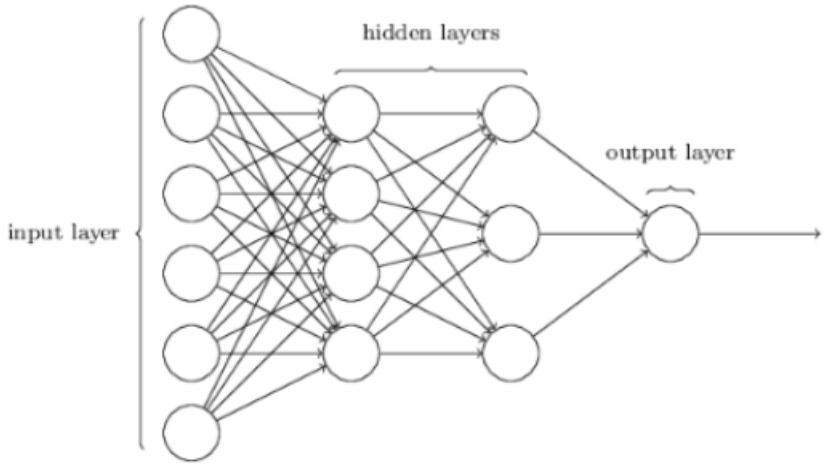

Figure 11: A densely connected, feed-forward, 3-layer, ANN [4]

output. At the final output layer, the model will output a prediction, $\hat{\mathbf{Y}}$, that will try to match the truth, $\mathbf{Y}$. This is where the error function, or loss, is calculated between the prediction, $\hat{\mathbf{Y}}$, and the truth, $\mathbf{Y}$. The initialized weights in each layer are rarely correct and will often result in a very high loss. After determining the loss, the back propagation algorithm determines the derivative of the loss with respect to the weights. The optimizer then updates the weights using the calculated derivative to follow the gradient down, hence the name *gradient descent*, and optimally reduces the loss for each batch in every epoch. Through this process, the model tries to find the Global Loss Minimum (GLM), although it usually ends up in a Local Loss Minimum (LLM) which is close enough to the GLM for practical purposes, which leads to the best approximation of the truth, $\mathbf{Y}$.

2.6.2 Types of Neural Networks

While machine learning is its own subset of artificial intelligence, neural networks are broken down further into three major types - Densely connected, feed-forward ANN, Recurrent Neural Network (RNN), and Convolutional Neural Network (CNN).

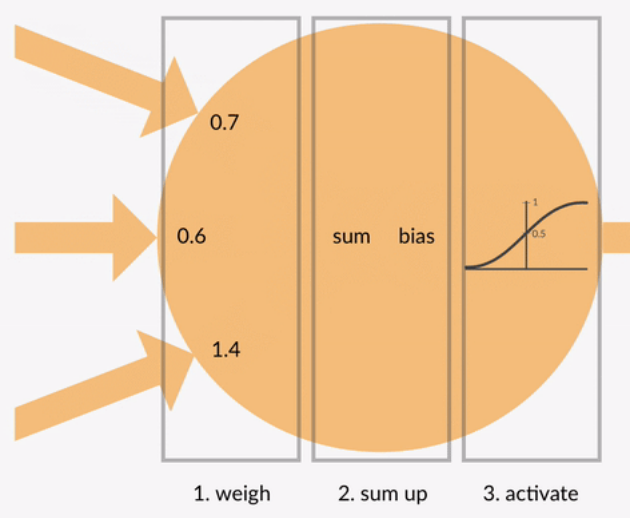

Figure 12: The process taking place inside of each neuron in a layer[5]

2.6.2.1 Artificial Neural Network

ANNs are sometimes referred to as "Universal Function Approximators" for their ability to map nearly any input to an output and work best with tabular data[21]. RNNs excel at classifying data that can only makes sense as time progresses, or in a sequence, such as speech. CNNs are the best choice for interpreting and classifying image data[22]. These different types of neural networks are separated by the structure in which they are created. Fig. 11 shows how a standard, densely connected, forward-feeding ANN would look. This dense configuration (all nodes in the current layer being connected to all nodes in the following layer) is not well suited to image classification. In this configuration, the pixels of an image would need to be flattened into a vector matrix. This image flattening is undesirable because it takes away any context between the rows and columns of an image. Certain features in an image, like the ears or snout of a dog, would lose their meaning if they get split up into a vector matrix. On top of that, large images would scale poorly and the network would have trouble finding features regarding the subject of the photo. Another weakness of ANNs comes from its lack of memory between samples in time

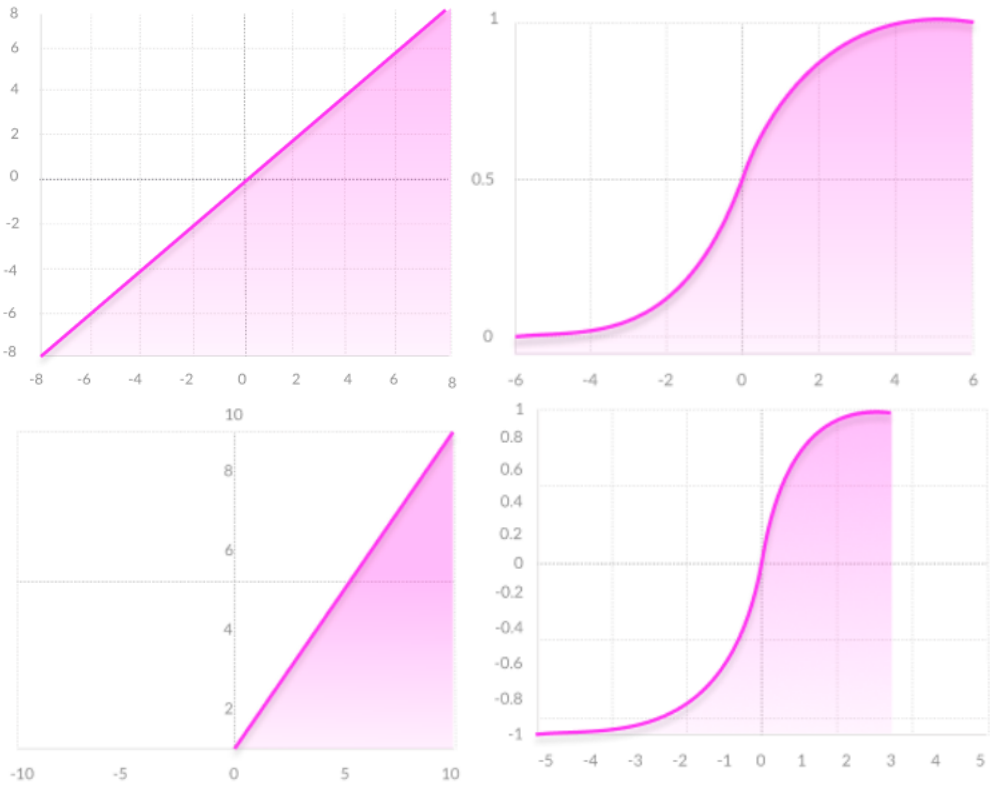

Figure 13: A series of common activation functions. Top Left: Linear. Top Right: Sigmoid. Bottom Left: ReLU. Bottom Right: TanH.[6]

and therefore cannot predict possible future inputs with while using previous outputs. RNNs and CNNs, while they have their own shortcomings, help alleviate the problems that ANNs encounter while training.

2.6.2.2 Recurrent Neural Network

As mentioned, RNNs excel at classifying data that makes sense as time continues. Figure 14 displays a simple RNN configuration. Here, the inclusion of *state t* into the activation function leading to *output t* allows the RNN to make a prediction based on input data from a previous time step. A very important feature that allows some measure of predicting sequential outputs. This basic model has the ability to scale

up to more robust versions such as an Long Short-Term Memory (LSTM) that, while adding to complexity, reduces or eliminates some of the common pitfalls of neural networks in general such as vanishing or exploding gradients[7].

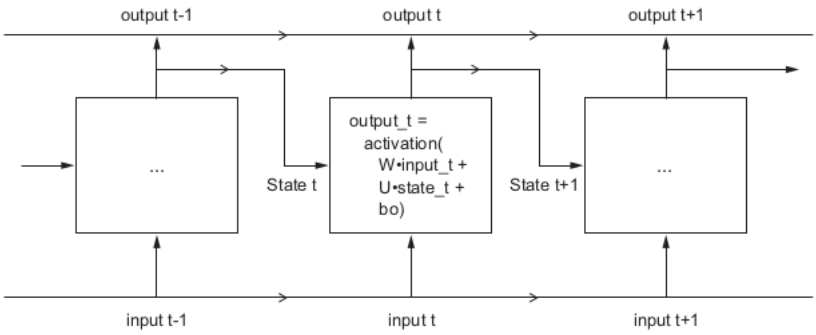

Figure 14: Basic RNN architecture[7]

2.6.2.3 Convolutional Neural Network

The final type of neural network is a CNN, specializing in the classification of images or detection of objects within an image. The architecture of a CNN is very unique compared to RNNs or ANNs. CNNs work by reducing an image to features within the image and classifying the image based on the probability of each feature, such as ears or snout of a dog, being present in a given classification[22]. A CNN breaks down a given image into convolutional kernels and pooling layers to help find such features.

In the case of the 2 Dimensional Convolutional Neural Network (2DCNN) shown in Figure 15 the kernel passes over the image in left-to-right, top-to-bottom manner. The value passed to the next convolutional layer is determined by the type of pooling done in the pooling layer. In the case of max pooling, the highest value in a kernel will be passed. Average pooling and min pooling act in the same manner. This convolution and pooling process is repeated until the image is reduced to a size more appropriate for classification at the output layer.

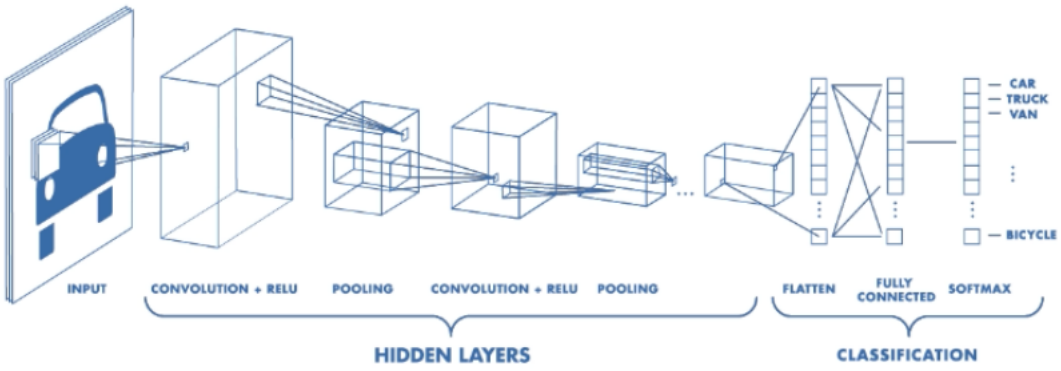

Figure 15: Process and architecture of a Convolutional Neural Network[8]

2.7 Recent Tolles-Lawson and Neural Network application to MagNav

The results of the two flights in Canciani's paper, detailed in chapter I, show that MagNav can a beneficial addition to Alternate Navigation (AltNav) as a whole in a GPS denied environment. The quality of magnetic maps is extremely important to MagNav and is currently an issue - but only because of the time-consuming and costly nature of collecting magnetic data. The process for collecting this data is effectively solved. Many aircraft, such as an F-16, in practical use can't operate with a boom on its exterior. To enable use of MagNav on an aircraft such as an F-16 the MagNav sensors would need to placed inside the hull of the aircraft. Doing this puts the MagNav sensors in much closer proximity to magnetic disturbance sources within the aircraft. The remaining problem that holds back fieldable use of MagNav is the current lack of a reliable method to calibrate MagNav sensors within an aircraft to filter out any potential aircraft disturbance. Initial steps to solve this problem were taken by Hezel[13]. A series of experiments with a small, wooden Unmanned Aerial Vehicle (UAV) with neodymium magnets placed on the control surfaces captured data that simulated the magnetic field of an airborne aircraft. There were four experiments in all. First, a "flight" complete with a simulated take off, normal flight, and a

simulated landing. Although the UAV never actually left the ground, this experiment aimed to capture the magnetic characteristics of a real airborne aircraft. Second, the aircraft remains stationary and is only rotated about that single point. This was in order to capture the change in DC levels of the aircraft disturbance field that change based on the aircraft's heading in relation to Earth's magnetic field. Experiment three was a repeat of the first however the engine was turned off in an effort to capture the disturbance field caused only by the moving control surfaces with magnets placed on them. Finally, the fourth experiment replicated the rectangular calibration pattern. Without turning the engine on, the aircraft was pushed through the pre-determined route and the control surfaces were manipulated by hand. The control surfaces were made to resemble the same oscillatory motion in the yaw, pitch, and roll axes that would be present in a powered, airborne rectangular calibration pattern.

These experiments collected data that would later be put through the traditional TL, ATL, and ANN algorithms. The dense ANN model won by a large margin by being able to predict the aircraft disturbance field to a mere 4.7nT RMSE. This is compared to traditional TL result of 47.0nT RMSE and Augmented Tolles-Lawson's slight improvement at 45.0nT RMSE. The reason TL and ATL struggled was determined to be their inability to predict the effect that moving control surfaces and aircraft subsystems had on the overall aircraft disturbance field. The movement of control surfaces as well as the change in aircraft disturbance field with respect to its orientation within Earth's magnetic field makes for a non-linear problem. Since the TL algorithm is a linear regression model, it cannot adequately model this problem whereas the dense ANN used could more easily model non-linearities with the implementation of their non-linear activation functions.

III. Methodology

3.1 Data

The data used for experimentation was collected at USAF Test Pilot School (TPS). The aircraft was an F-16. A pod was attached under the wing of the F-16 with a series of 3 vector magnetometers, 4 scalar magnetometers, 2 inertial measurement units, and a GPS receiver. Along with this set of sensors, data was collected that describes the usage of various subsystems within the aircraft. With a set of magnetic survey maps, collected by survey aircraft for the sole purpose of serving these experiments, these are all the tools needed in order to perform calibration experiments with TL, ATL, Artificial Neural Networks.

There are multiple days and flights over which this data was collected. The typical structure of a single flight can be seen in Figure 16. On a day in which data was collected, there were either one or two total flights. Within a single flight there were up to two patterns flown. These patterns were flown with either the purpose of calibration or navigation in mind. Calibration flights, like the rectangular and cloverleaf patterns are flown in order to provide data sets for standard Tolles-Lawson (TL) calibration.

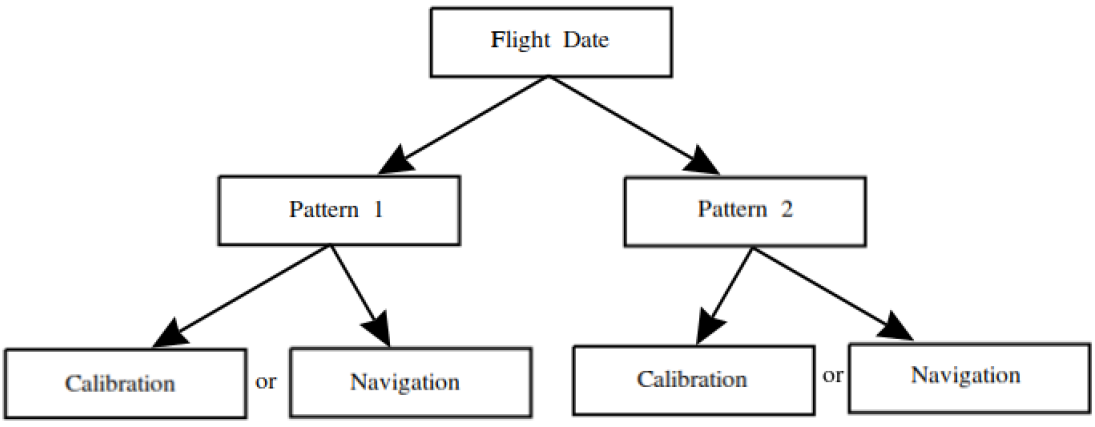

Figure 16: The structure of data from a single flight performed by the F-16

Navigation flights come in the form of 2D maneuvers (patterns flown at a single altitude) or in the form of 3D maneuvers (patterns flown at varying altitudes). While navigation flights will be used for training ANNs, they are not expected to perform better because navigation flights lack information that can help describe the aircraft disturbance field in the same way as calibration flights. Navigation flights stand to emulate real world flight in order to test the capabilities of the models trained on calibration flights.

3.2 Experimental Design

Given that the flight patterns are flown at a sufficient altitude from ground magnetic sources like power lines, typically operating at in the same designated frequency band as rectangular calibration maneuvers at 60Hz, the only magnetic signal present in the measurements comes from Earth's core field, Earth's crustal field, Solar Quiet currents (SQs), and the aircraft disturbance field[13]. The Earth's core field is estimated easily with an Earth magnetic reference field since its intensity does not change much within a local area. Within the confines of the data used in following experiments, the test area is so small that the Earth's core field does not vary and only acts as a scalar bias in measurements. This is the point when SQ current's would be removed as well. However, as an oversight with the received data, SQ currents were not removed because it was believed to have already been compensated for at the time of data collection. By the time this was noticed, it was too late to make the necessary changes. The only data left to model at this stage, is Earth's crustal field and the aircraft disturbance field. Although ANNs have already been shown to model the aircraft disturbance field better than TL and ATL, the traditional methods do still hold a purpose for upcoming experiments[13]. Utilizing TL will help determine more effective augmentations in ATL. The beneficial augmentations found through ATL

will be the augmentations used in accompanying artificial neural network models.

3.3 Experiment Environment

Smaller experiments are conducted on a Lenovo ThinkPad with an Intel core I7 vPro 8th Gen CPU with 12 cores at 4.3GHz, 46GB DDR4 RAM, and an NVIDIA Quadro P3200 GPU. For more resource intensive experiments like deep networks, networked computers within the Autonomy and Navigation Technology (ANT) center at the Air Force Institute of Technology (AFIT) are used. These networked computers have access to much more powerful CPUs with more cores, larger pools of RAM and sometimes multiple graphics cards in order to run numerous experiments at once and in lesser time.

3.4 Artificial Neural Network Models

Many of the beneficial aspects of model architecture and hyperparameters that were learned from Hezel's 2020 thesis will be carried over to these models as a starting point. Aspects such as a 32 batch size, TanH activation function, and relatively small layer sizes. The learning rates will start at $1e^{-4}$ and reduce by a factor of 0.8 when the validation loss plateaus after 10 epochs to a minimum learning rate of $1e^{-10}$. Many of the changes will most likely revolve around layer sizes, model depths, and total number of epochs.

Two types of artificial neural networks will be tested. The first will be a densely connected ANN that takes a single input model, in the form of either 18 traditional TL parameters or 18 TL parameters + N augmentations, which outputs a single output that represents the models best approximation of the aircraft disturbance field. This model architecture can be seen below in Figure 17 and will be referred to simply as the single input model.

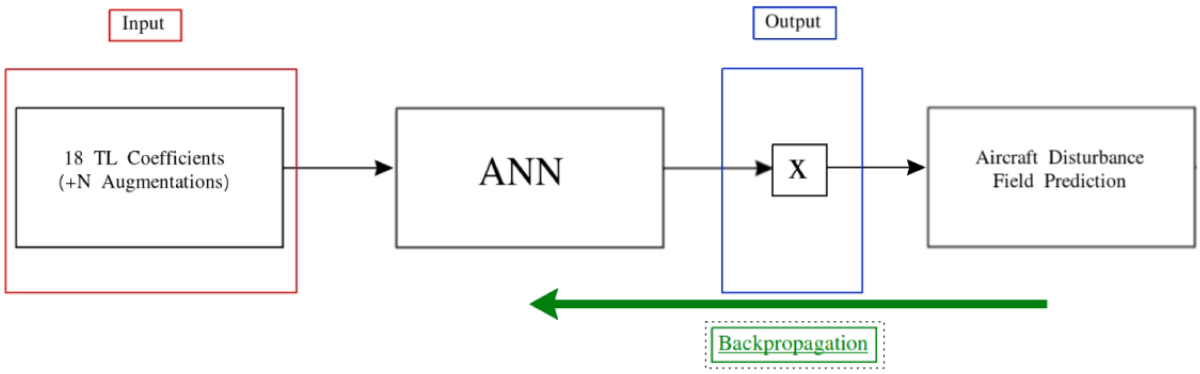

Figure 17: Single input, single output model architecture.

The second model attempts to mix the filtering properties of TL with the non-linear capabilities of a densely connected ANN and is called the Mixing Artificial Neural Network and Tolles-Lawson (MANNTL) model. This model can be visualized in Figure 18. This model utilizes two inputs - one unfiltered set of data and one filtered set of the same data. Although, the model will still output a single value that represents its best approximation of the aircraft magnetic disturbance field. Aside from two inputs, another major difference is the size of the output layer. In the single input model, the output of the ANN model was a scalar but the ANN within the MANNTL model outputs a vector matrix X. In the initial forward-propagation step, the X matrix is only influenced by the unfiltered data being fed to the ANN. In this way, it is no different from the single input model. However, the addition of the dot product is an important design aspect of the MANNTL model. Since the dot operation takes place within the model, and right before outputting its final estimation, the X vector and the model weights are influenced by the filtered data in the back propagation step. This process can be visualized in Figure 18.

Both the filtered and unfiltered data will be normalized by the same scale. This uniform normalization will help when scaling the models estimation back to normal values for evaluation purposes. This is also necessary because the model will not

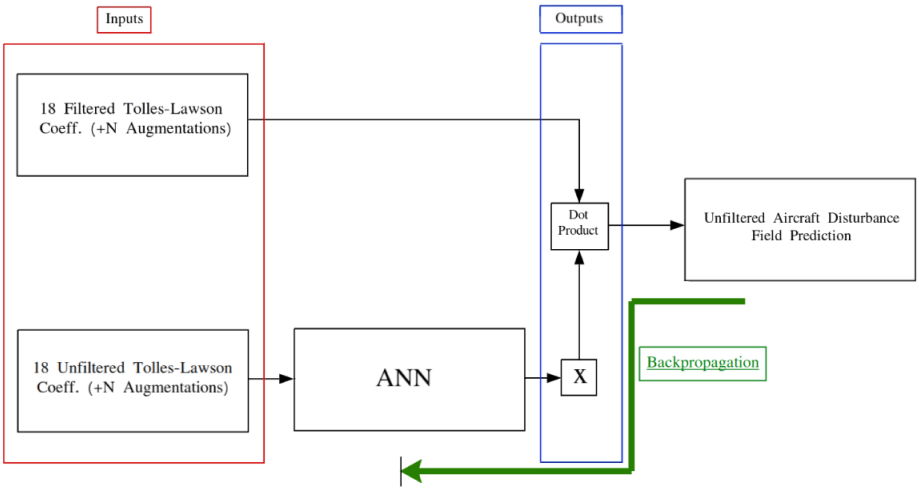

Figure 18: MANNTL model using filtered data as well as unfiltered data as inputs.

always have access to filtered data. Filtered data is only used when training and only serves to influence the weights and X vector of the model. In real world application the pilot will only have access to unfiltered data. This is why when evaluating the model, in Chapter IV, both inputs will be the same set of unfiltered data. A final important note is that both inputs will be scaled by the same normalization. This will make re-scaling the data at the output easier to manage.

3.5 Conclusion

This section covered the structure of the data used for experiments as well as the ANN models that will be experimented on. The data received was collected by Air Force TPS pilots with the sole purpose of magnetic calibration for the F-16 aircraft. To date, this is the most fully realized data set that aims to further general magnetic calibration methods. The first model discussed as well as the MANNTL model aim to fully explore the limits of magnetic calibration.

IV. Results and Analysis

4.1 Introduction

Explored in this chapter are the various experiments conducted on the available F-16 data provided by the Air Force TPS. With such data diversity in collected data, the most important step to take is defining the data used in each experiment. The separation of data and will provide splitting of data that ensures there is no mixing between training, validation, and test sets for all experiments. The next topic covered here in Chapter IV are the breakdown of experiments. First are the findings of traditional Tolles-Lawson (TL) - constructing the 18 columns of data that model the aircraft permanent, induced, and eddy current magnetic disturbance fields then subsequently filtering that same data and fitting the model. Second, using the same 18 filtered TL columns as well as a combination of **N** augmentations for Augmented Tolles-Lawson (ATL) will be performed. Finally, using the same 18 TL columns and ATL augmentations, a series of test will be performed on the single input model resembling that of Hezel's[13] model as well as the newly developed MANNTL model. Results found in each of these sections will be discussed and broken down in each of their respective sections.

4.2 TL and ATL Test Data

Starting with the Tolles-Lawson data in Table 1, these flights were selected because they were specifically flown with TL in mind. This is apparent because of the height above Mean Sea Level (MSL) they were flown, 9,000m. Given the height of the provided maps for experimental use, 1,200m and 5,400m, truth data cannot be generated for training even with upward continuation at 9,000m. This is not a problem for TL because after filtering at the prescribed 60Hz band, the only content remaining

in the magnetometer data is that of the aircraft disturbance field, as noted in Section 2.4. To see how this performs on navigation flights though, truth data is needed to compare the results to. The test data in Table 1 was flown at a much lower altitude, 5,400m. This altitude allows for the generation of truth data with the provided maps via interval continuation.

Table 1: Tolles-Lawson Test data Splits

Training				
September, 2020 Flight Date(Flt)	Altitude(m) above MSL	Pattern Type	Desc. (MagEnv)	Samples (20Hz)
17(1)	9,000	Calibration	Rectangular (Q/L)	24,000
18(2)	9,000	Calibration	Cloverleaf (Q/L)	27,000
Test				
September, 2020 Flight Date(Flt)	Altitude(m) above MSL	Pattern Type	Desc. (MagEnv)	Samples (20Hz)
17(1)	5,400	Navigation	2D Maneuvers (Q)	24,000
18(2)	5,400	Navigation	2D Maneuvers (Q)	27,000

These flights serve as the optimal conditions for TL and ATL aside from breaking the Tolles-Lawson assumptions #1, that the aircraft field is negligible compared to the earth field, and #2, that the earth total field is roughly equivalent to Earth's core field. For more detail, see section 2.4. Keep in mind, there is no validation set for these algorithms for two reasons. First, the data received did not allow for a validation set of data that catered to TL. Second, these algorithms are well documented and there is not any real room for improvement to warrant validation experiments anyway.

4.3 TL and ATL Test Results

Training data	Test data	TL RMSE(nT)	ATL RMSE(nT)
Sep 17 Rectangular(Q/L)	Sep 17 2D Maneuvers(Q)	6.94	7.02
Sep 18 Cloverleaf(Q/L)	Sep 18 2D Maneuvers(Q)	45.75	45.08

Table 2: Results from TL and ATL algorithm testing.

Table 2 shows that augmentations deemed *beneficial* by the ATL algorithm do not help very much. In fact, the ATL algorithm performed slightly worse than the TL algorithm when trained on the Sep 17 rectangular flight data. The implication that ATL chosen augmentations do not help model the aircraft disturbance field will be supported by results in the later ANN models.

4.4 ANN Training, Validation and Test data

In upcoming tests aimed at optimizing the ANN models, TL and ATL will be performed but these data sets will not cater to TL in the same way. This is because ANN models require truth data for not only validation and test sets but also for training. Below in Tables 3 and 4 are the training, validation, and tests sets. The large differences between these training sets and the ones from Section 4.2 is the altitude. As mentioned, if collected data falls between the altitudes of 1,200m and 5,486m, interval continuation can be performed and truth data can be interpolated. The calibration flights all take place at 5,400m altitude.

Important to note as well is the Magnetic Environment (MagEnv) column denoted in Tables 1, 3, and 4. MagEnv denotes whether or not the F-16s Radio Detection and Ranging (RADAR) system is on or off. If MagEnv is labeled Q, quiet, RADAR is off. If labeled L, loud, RADAR is toggled on. Q/L is used for when only a portion of the flight has RADAR toggled off, and the rest it is toggled on.

Table 3: Training and Validation data split for ANNs

Training				
September, 2020 Flight Date(Flt)	Altitude(m) above MSL	Pattern Type	Desc. (MagEnv)	Samples (20Hz)
9(2)	5,400	Calibration	Rectangular (Q/L)	26,000
9(2)	5,400	Calibration	Cloverleaf (Q/L)	36,000
Validation				
September, 2020 Flight Date(Flt)	Altitude(m) above MSL	Pattern Type	Desc. (MagEnv)	Sample s(20Hz)
10(2)	2,100	Navigation	2D Maneuvers (Q)	42,000
10(2)	2,100	Navigation	2D Maneuvers (L)	36,000
11	2,100 - 5,400	Navigation	3D Maneuvers (Q)	68,000

Table 4: Training and Test data split for ANNs

Training				
September, 2020 Flight Date(Flt)	Altitude(m) above MSL	Pattern Type	Desc. (MagEnv)	Samples (20Hz)
16(1)	5,400	Calibration	Rectangular (Q/L)	21,000
16(1)	5,400	Calibration	Cloverleaf (Q/L)	51,000
Test				
September, 2020 Flight Date(Flt)	Altitude(m) above MSL	Pattern Type	Desc. (MagEnv)	Samples (20Hz)
17(1)	2,400	Navigation	2D Maneuvers (Q)	30,000
18(2)	2,400	Navigation	2D Maneuvers (Q)	48,000
16(2)	2,100 - 5,400	Navigation	3D Maneuvers (Q/L)	76,000
21	2,100 - 5,400	Navigation	3D Maneuvers (Q/L)	68,000

4.5 ANN breakdown

For both the Single input model and the MANNTL model there will be 5 experiments conducted. The 5 experiments are broken down into an itemized list below.

- **Experiment 1:** The model will be trained on the first 98% of samples within a flight, calibration or navigation, and will be validated on the remaining 2% of the same flight. Every layer in the ANN model will have **18** neurons, one neuron for each column of data from TL equations. The aim of this experiment is to test the models ability to predict the aircraft disturbance field should the pilot fly a quick calibration flight at the start of a sortie then continue as normal. This is inspired by the experiment performed in Hezel's thesis[13].

- **Experiment 2:** The model will be trained on a full rectangular calibration flight and validated on a series of navigation flights that are performed on a later date. Every layer in the ANN model will have **18** neurons, one neuron for each column of data from TL equations. The aim of this experiment is to gauge the models ability to predict the aircraft disturbance field a few days after calibration while only using the 18 TL equations. Should models be able to hold up over the course of a week or two this will save the pilot fuel and time in the long run.

- **Experiment 3:** The model will be trained on a full rectangular calibration flight and validated on a series of navigation flights that are performed on a later date. 4 Augmentations will be added to this model making the size of each layer in the ANN model **22** neurons. Augmentations will be chosen by running the ATL algorithm. The combination of 4 augmentations that performs best with the ATL model will be used in ANN model. The aim of this experiment is to gauge the models ability to predict the aircraft disturbance field a few days

after calibration while using the 18 TL equations as well as augmenting data.

- **Experiment 4:** This experiment is the same as experiment 2. The only difference being that the model will be trained on a full cloverleaf calibration flight instead of a rectangular calibration flight.

- **Experiment 5:** The model will be trained on a full cloverleaf calibration flight and validated on a series of navigation flights that are performed on a later date. Every layer in the ANN model will have **54** neurons. The model will only receive data created by the 18 TL equations. The aim of this experiment is to gauge how well a model can predict the aircraft disturbance field over the coarse of a few days when given more flexibility in each layer.

Each of these experiments will be performed twice. Once for both the single input model as well as the MANNTL model. For the sake of organization and brevity, these experiments will be referred to as "single input experiment 1" or "MANNTL experiment 3" in the coming sections. In each results section there will be two plots. One showing how the model performed on the training data, and one showing how the model performed on validation/test data.

From the results displayed in Hezel's thesis [13], it is expected that hyperparameters won't play as much of a role in reducing RMSE nearly as much as the depth of the neural network and the sizes of each layer. For this reason, the following ANN tests will be focused on changing model depth and layer size as well as adding augmentations to try to find trends that reduce overall RMSE.

All models were trained to a point where they could not learn anything more about training data. Often times this led to overfitting as can be seen in Figure 19.

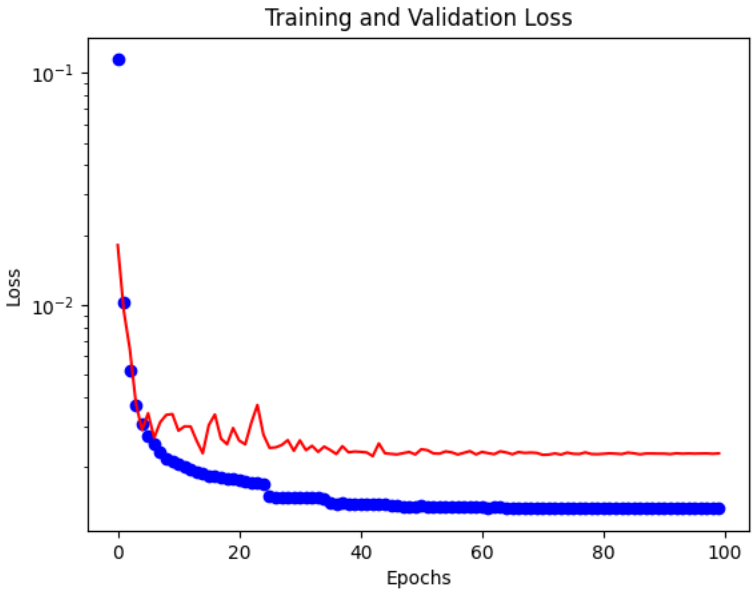

Figure 19: Plot of the loss over the course of training the MANNTL model. 100 Epochs, No regularization, Learning rate minimum reached.

In early models, regularization was added as a means to fight overfitting. While regularization, like dropout, did help fight overfitting it also worsened the models ability to predict on validation data. Models shown in the coming sections will *not* utilize regularization for this reason.

Hyperparameters for the model will remain consistent across all experiments. TanH activation function, 32 batch size, and a learning rate that starts at $10e^{-4}$ and reduces to $10e^{-10}$ as training progresses. The learning rate will be set to drop by a factor of 0.8 when the loss plateaus for 10 epochs. In the beginning stages of training the model, dropping the learning rate can have a drastic effect as can be seen at the 35 epoch mark in Figure 19. Further into training though, the model is reaching either the GLM or LLM and learning rate drops become less effective.

4.6 Neural Network Validation Results

4.6.1 Single input ANN Results - Validation

The single input model is the architecture built to resemble the model from Hezel's thesis. The training and validation set results are shown below.

4.6.1.1 Single Input Experiment 1 Results - Validation

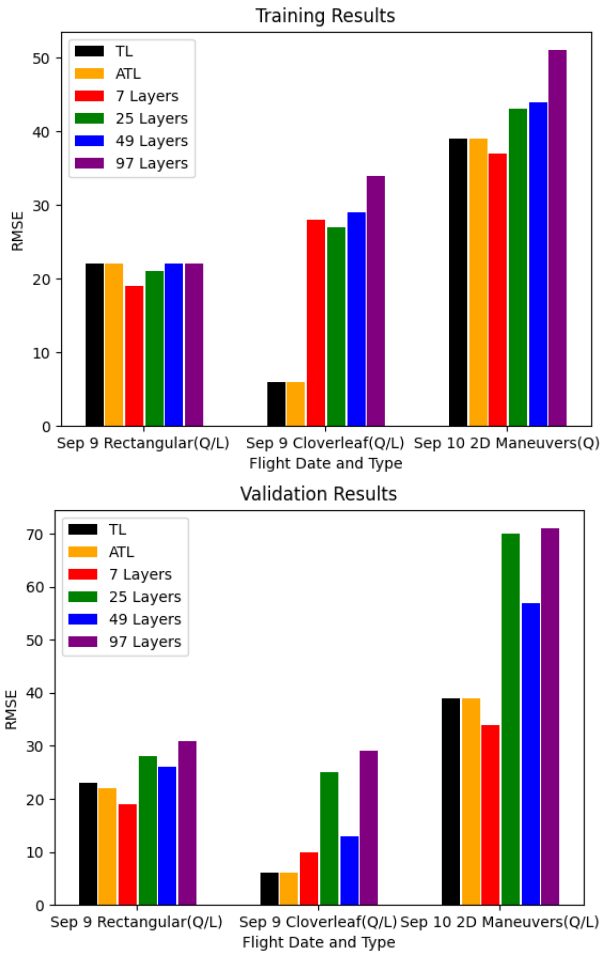

Figure 20: Results for Single Input Experiment 1. 300 Epochs

4.6.1.2 Single Input Experiment 2 Results - Validation

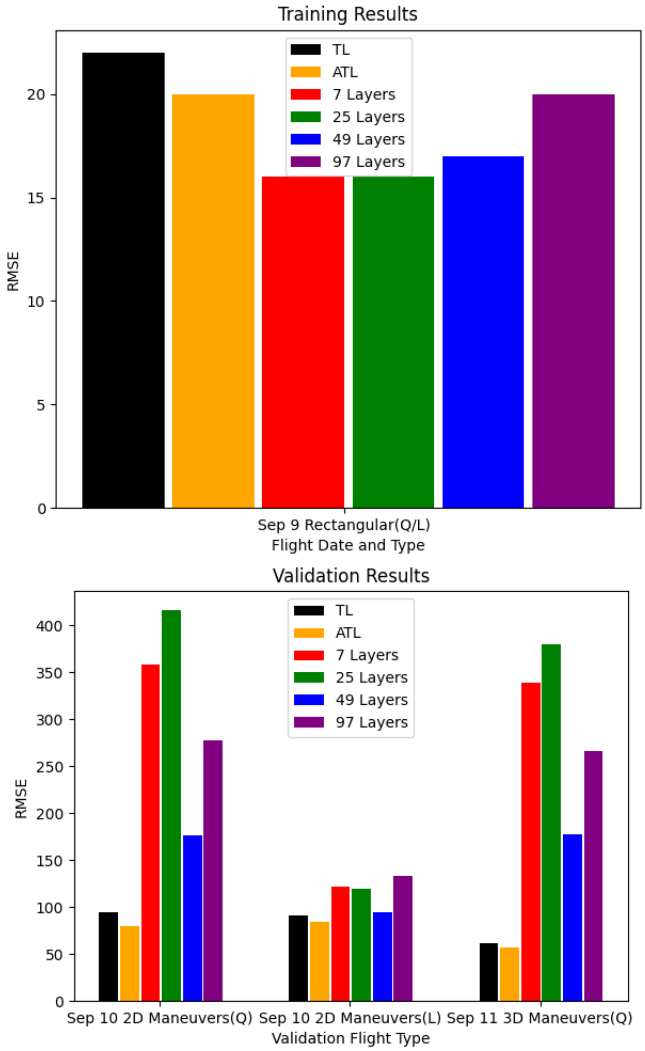

Figure 21: Results for Single Input Experiment 2. 300 Epochs

Notice the change in the training bar plot here. This is different from Figure 20 training because the models in this experiment were only trained on rectangular calibration data. These models were then validated on the three navigation flights in the bar plot detailing validation results.

4.6.1.3 Single Input Experiment 3 Results - Validation

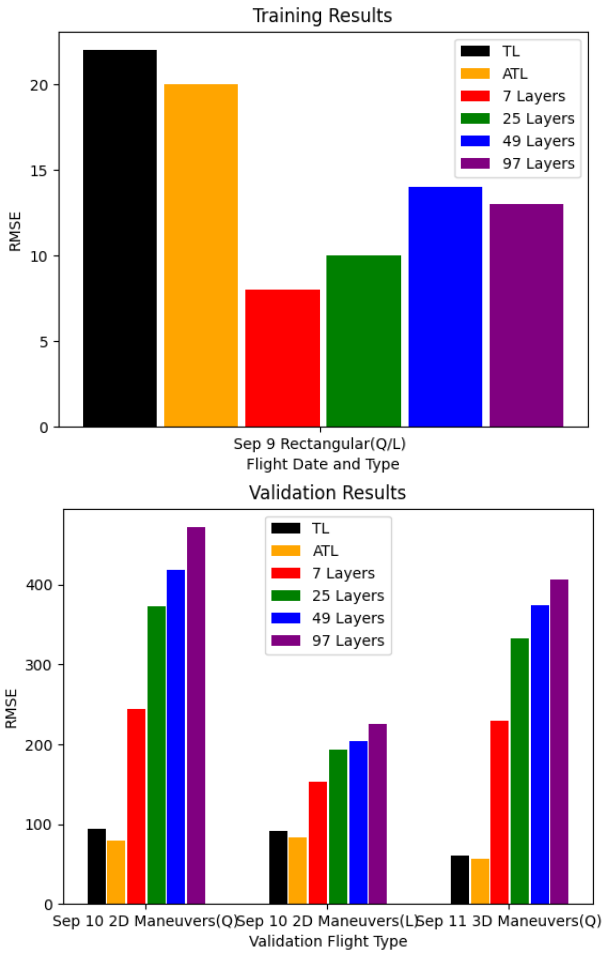

Figure 22: Results for Single Input Experiment 3. 300 Epochs

4.6.1.4 Single Input Experiment 4 Results - Validation

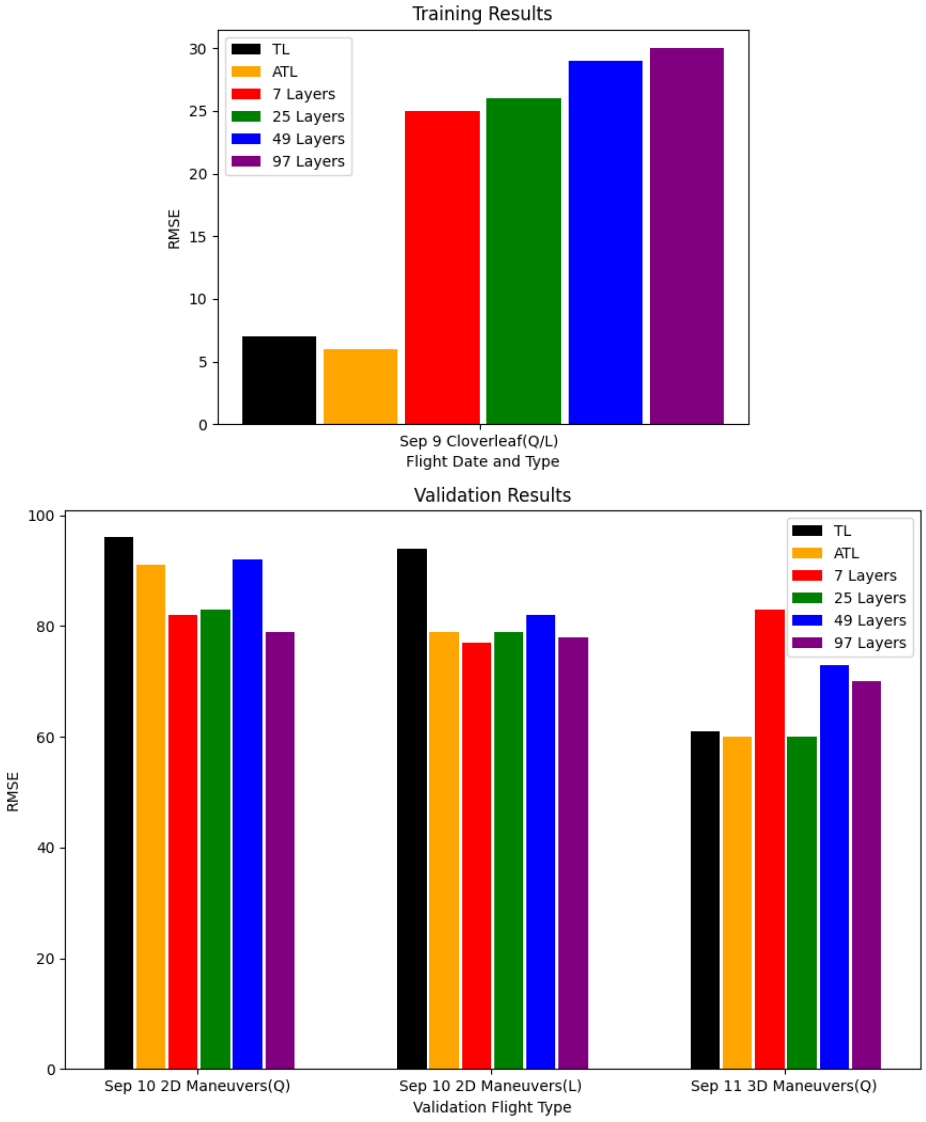

Figure 23: Results for Single Input Experiment 4. 300 Epochs

4.6.1.5 Single Input Experiment 5 Results - Validation

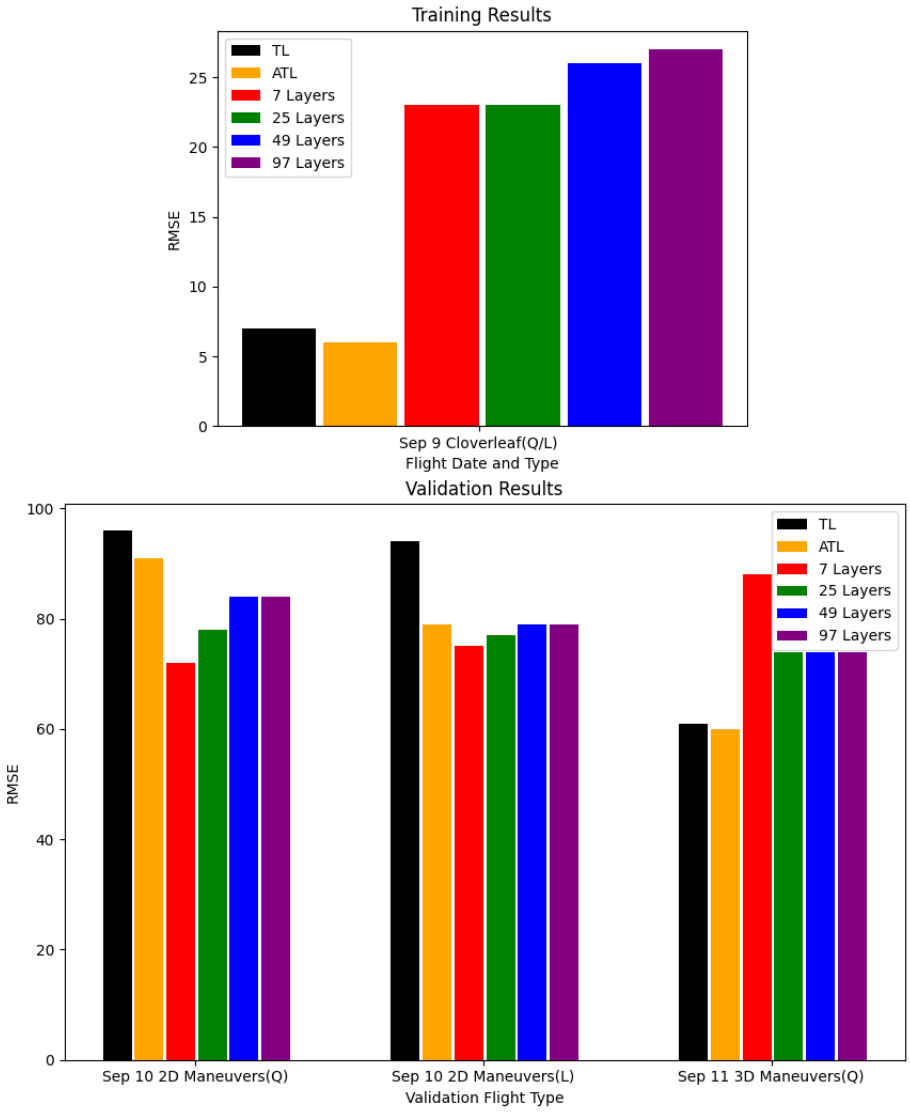

Figure 24: Results for Single Input Experiment 5. 300 Epochs

4.6.1.6 Single Input Results Analysis - Validation

In general, the single input model preferred shallower models. In nearly all cases, the 7 layer models performed the best. Perhaps removing layers and training models on only 2-5 layers would be even more beneficial.

From Figures 21 and 23, it can be seen that single input experiment 4 was more

effective single input experiment 2. However, the opposite is true of the training results. The model was able to memorize the rectangular pattern (experiment 2) data better than the cloverleaf pattern (experiment 4). This memorization of rectangular pattern data is the most likely reason for worse generalization in the models from single input experiment 2.

Interesting results came from the single input experiment 3. Results from Figure 22 show that models augmented with extra sensor data performed much better when training. However, when it came to validation, the results are much worse. The likely cause is the way augmentation combinations were selected with ATL. In Hezel's paper, augmentation data was mostly describing the magnetic noise created by the control surfaces moving on the aircraft and this yielded great results[23]. However, when the ATL algorithm was left to choose its own augmentation data that, it found beneficial, it may have never chosen the data describing control surface movement. Instead, the ATL algorithm may have chosen augmentations that were present and helpful for training, but were mostly absent in the validation data leading to reduced effectiveness of selected augmentations.

From experiment 5, widening layers marginally improved results in both training and validation. In the 7 layer model, training accuracy improved from 25nT to 20nT. Similar results can be seen in the 25, 49, and 97 layer models as well. In validation, these improvements really only carried over when predicting the quiet(Q) 2D maneuver set though.

When considering the MagEnv of the validation flights, models from experiments 2 and 3 performed much better on loud(L) flights. (L) denoting that radar was turned on for the entire flight. Both the rectangular pattern data and cloverleaf pattern data contain portions of the flight when radar was on and when radar was off, denoted (Q/L). Documentation on when the RADAR was on and when the RADAR was

off is scarce in supplementary documents though. So as speculation, rectangular pattern data could contain more data describing the effects of RADAR on the aircraft disturbance field - leading to better prediction in validation.

4.6.2 MANNTL model

The MANNTL model was developed to try to mix the strengths of both the TL algorithm and ANNs as explained in Section 3.4. In order to test the ability of the MANNTL model, the same experiments from 4.6.1 were performed and the only major change to the models were the required number of epochs need to train them. In general, the MANNTL model needed fewer epochs to learn all it could about the given data.

4.6.2.1 MANNTL Experiment 1 Results - Validation

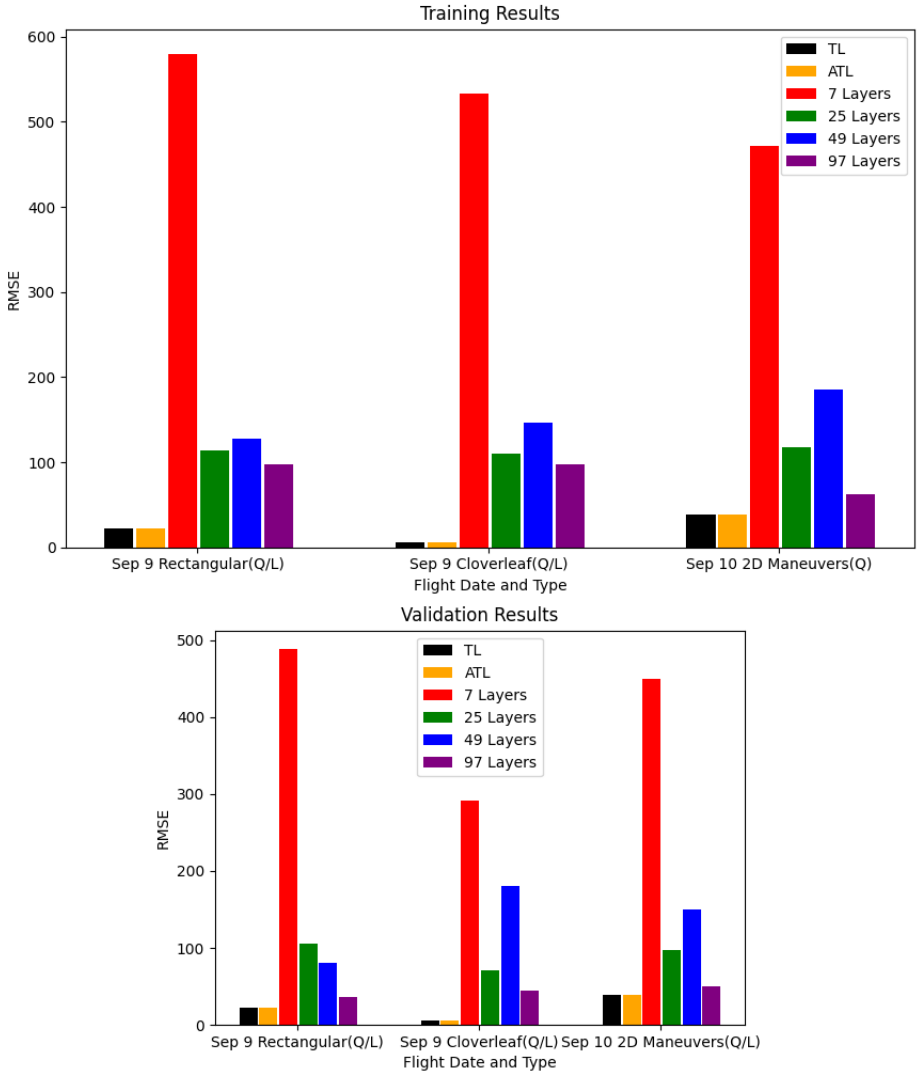

Figure 25: Results for MANNTL experiment 1. 100 epochs

4.6.2.2 MANNTL Experiment 2 Results - Validation

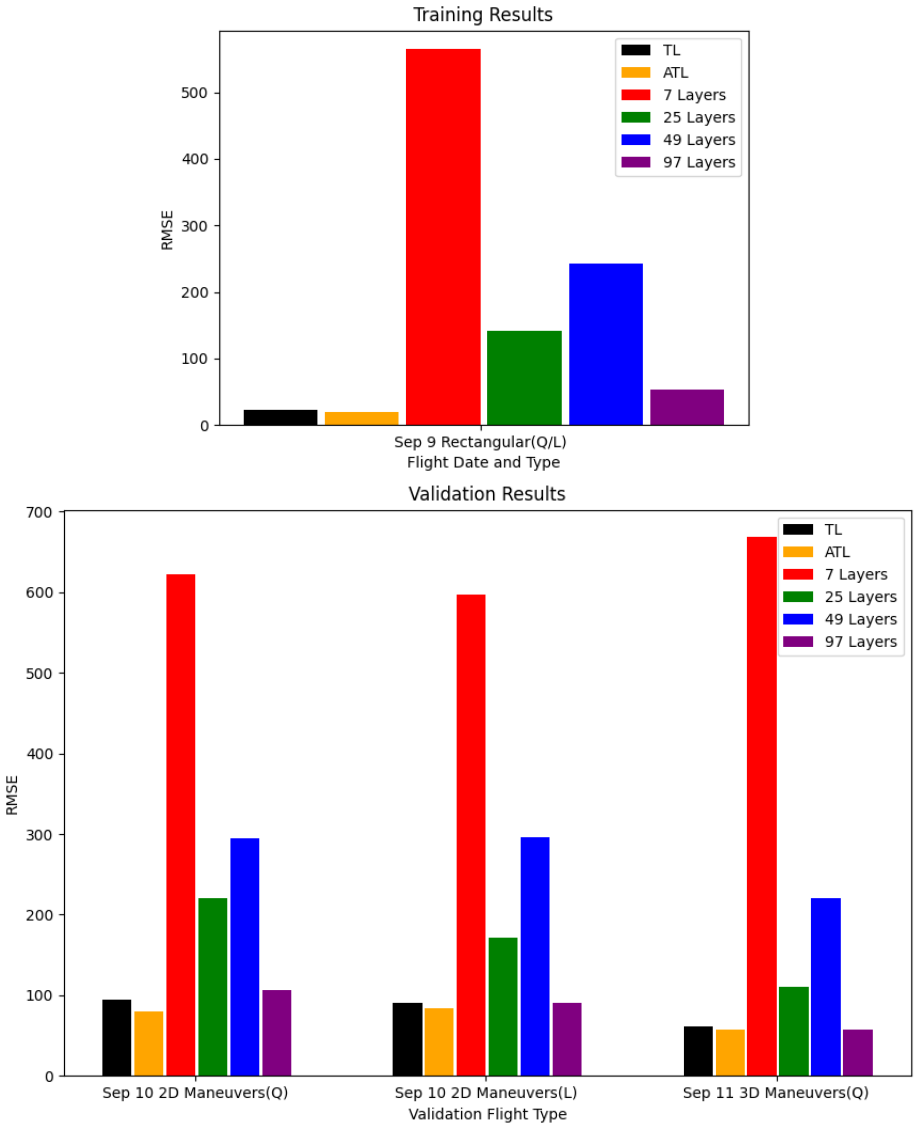

Figure 26: Results for MANNTL experiment 2. 100 epochs

4.6.2.3 MANNTL Experiment 3 Results - Validation

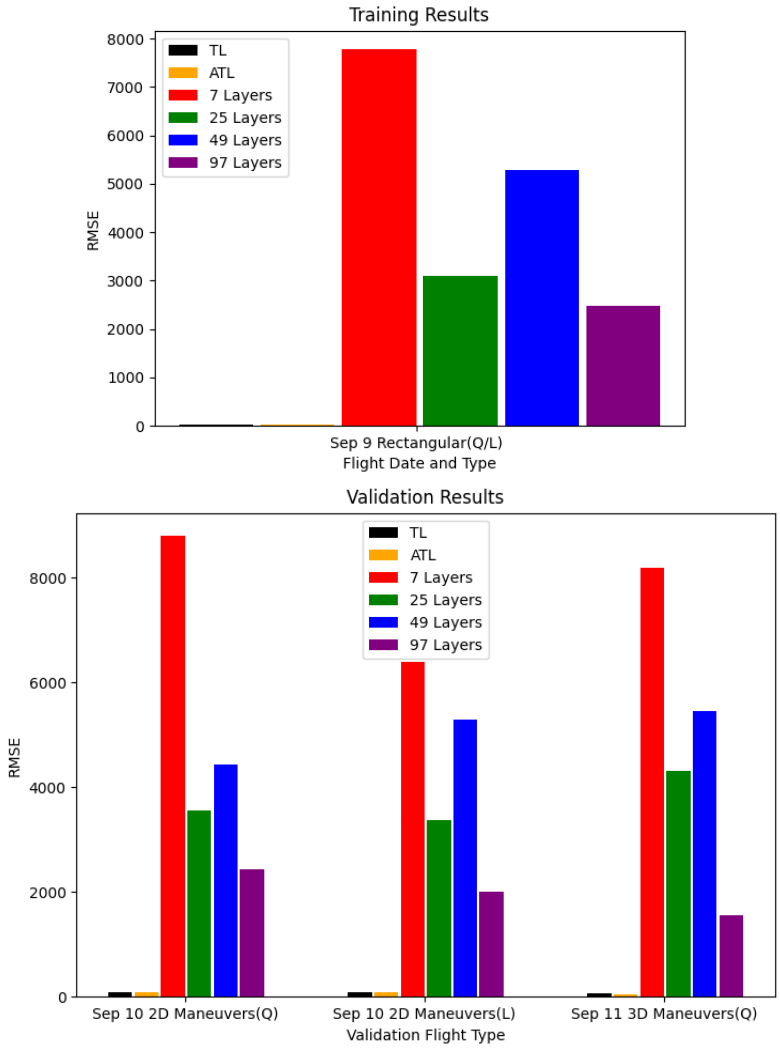

Figure 27: Results for MANNTL experiment 3. 100 epochs

4.6.2.4 MANNTL Experiment 4 Results - Validation

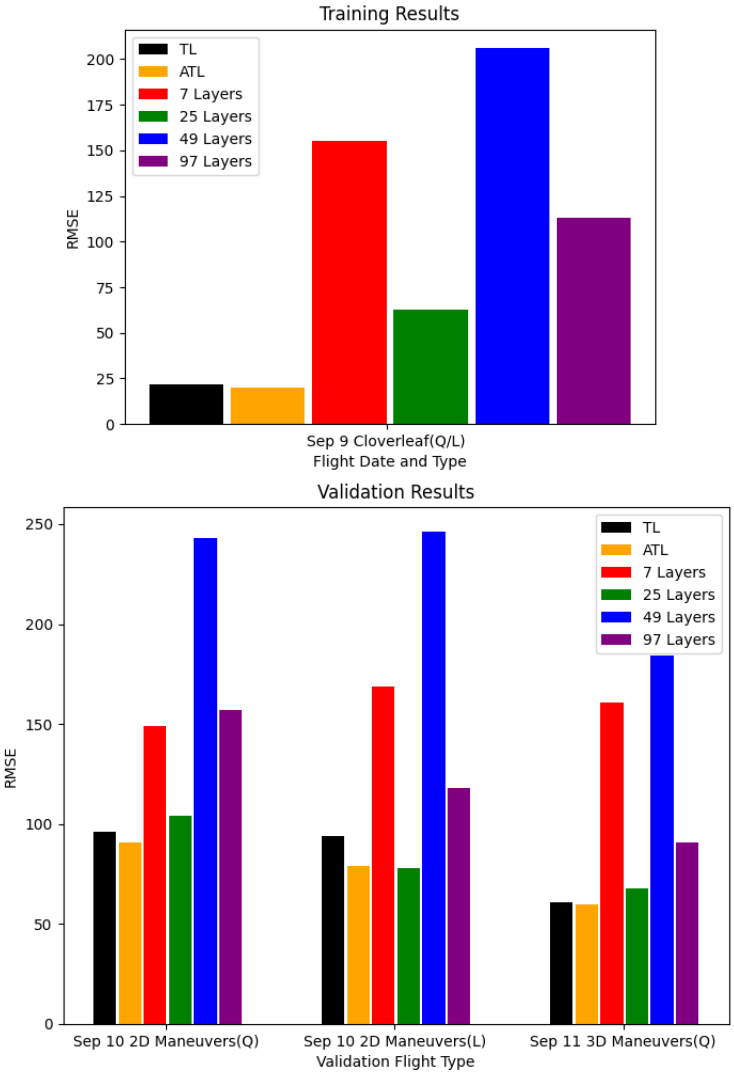

Figure 28: Results for MANNTL experiment 4. 100 epochs

4.6.2.5 MANNTL Experiment 5 Results - Validation

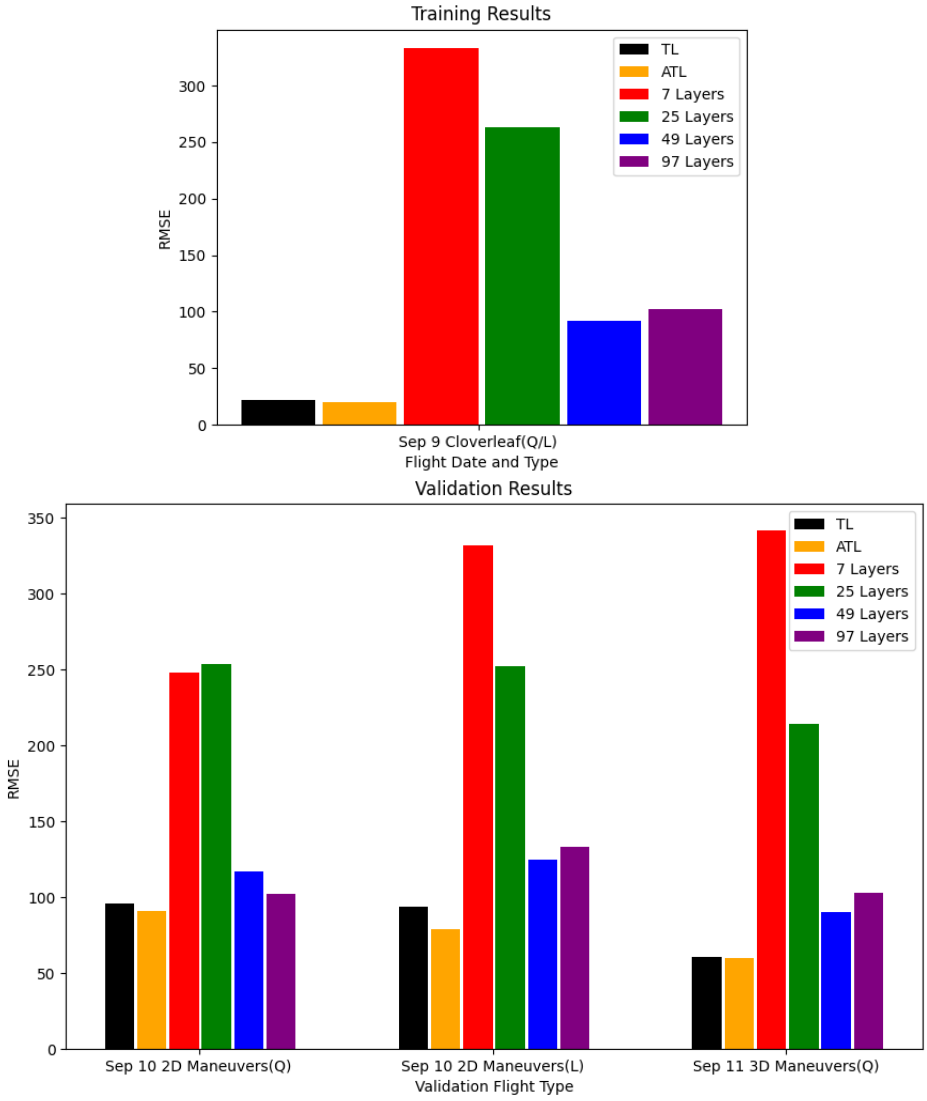

Figure 29: Results for MANNTL experiment 5. 100 epochs

4.6.2.6 MANNTL Results Analysis - Validation

The MANNTL model shows preference for deeper models such as with 97 layers. In all 5 experiments performed on the MANNTL model, the performance of the model in training is generally proportional to the performance in validation. However, no model in any experiment comes close to the performance of traditional calibra-

tion methods when training. In validation, there are a few models that can match traditional calibration but the overwhelming majority do not come close either.

When comparing the results from Figure 27 and 22. The effects of augmentations on training are opposite. MANNTL experiment 3 shows that the addition of augmentations selected by ATL make modelling the aircraft disturbance field impossible. From Figures 28 and 29, widening of the layers seems to solidify the effects of a deeper model.

4.7 Neural Network Test Results

Test models chosen for each of the 10 experiments conducted in Section 4.6 are based on consistency. All 5 of the experiment conducted with the single input architecture in general preferred more shallow networks at 7 layers. Whereas the MANNTL models preferred 97 layers of depth. The test models for single input and MANNTL models will reflect these preferences going forward.

4.7.1 Single Input ANN Results - Test

Figures 30 and 31 show that the test results mirror the validation results. Experiment 2, trained on rectangular data, performs worse than experiment 4, trained on cloverleaf data. Experiment 3 trained with augmentation data performs much worse overall. Experiment 5 shows negligible improvement over experiment 4.

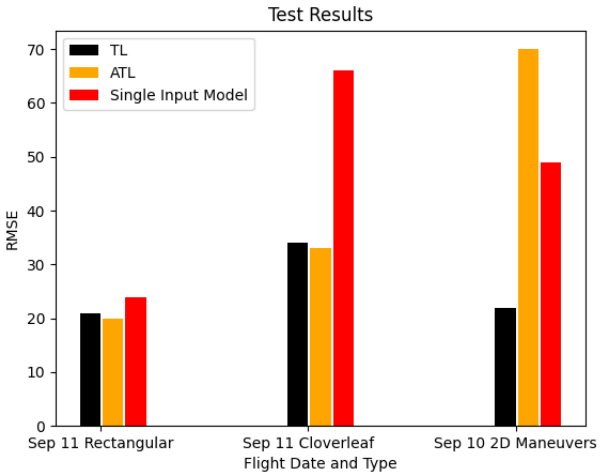

Figure 30: Test results for single input experiment 1. 7 layers, 300 epochs.

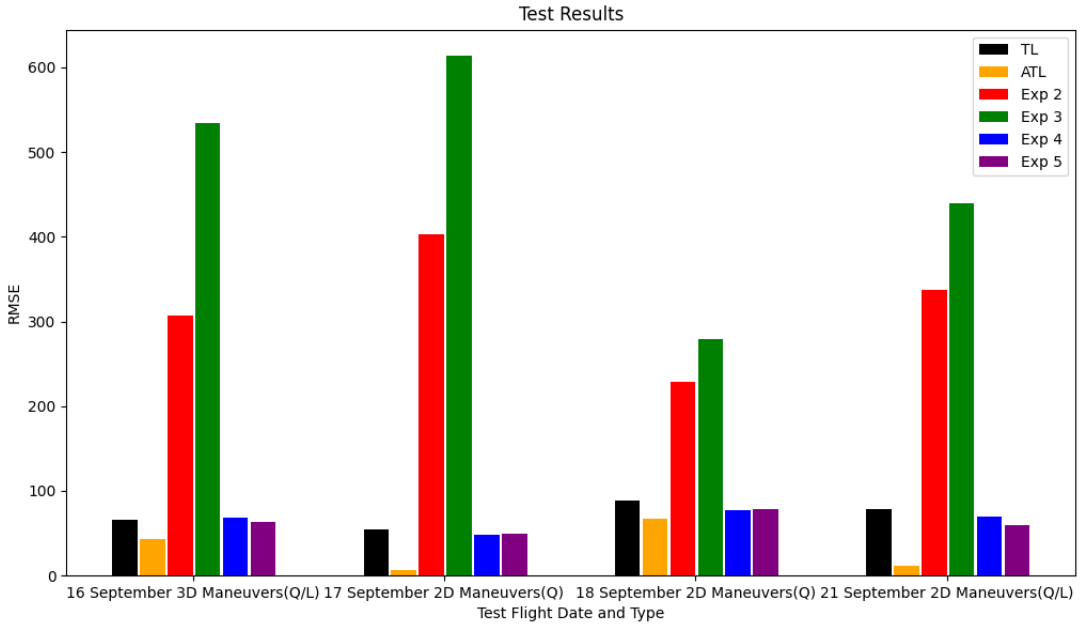

Figure 31: Test results for single input experiments 2-5. 7 layers, 300 epochs.

While the RMSE metric is helpful in determining overall ability of the models. Looking at plots that show what the single input model actually predicted in these cases is helpful in determining why the models may not have performed well. Figure 32 shows the prediction plots for single input experiment 2, tested on the 2D maneu-

ver flight from September 17. From Figure 32 it can be seen that when the aircraft disturbance field was relatively stable, the model could predict within a 100nT accuracy. However, when large swings were present the model had a very hard time predicting such movements and led to huge error spikes on the scale of 1000s of nT that had a hand in making the overall RMSE calculation worse.

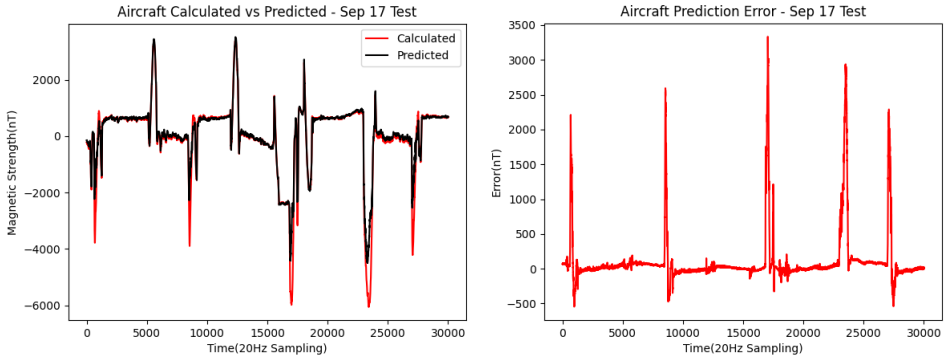

Figure 32: Prediction results single input experiment 2, tested on September 17 2D maneuver flight. Left: Predicted vs. calculated aircraft disturbance field. Right: Error in aircraft disturbance field prediction

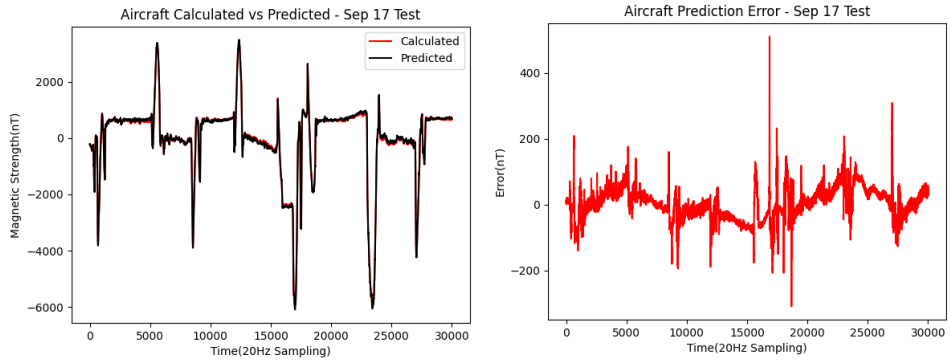

Figure 33: Prediction results for single input experiment 4, tested on September 17 2D maneuver flight. Left: Predicted vs. calculated aircraft disturbance field. Right: Error in aircraft disturbance field prediction

These large prediction errors are not present in Figure 33 which shows predic-

tion results from single input experiment 4, tested on the same 2D maneuver from September 17. This models ability to predict these large swings, where the model trained on the rectangular could not, makes for a much more accurate prediction of the aircraft disturbance field.

4.7.2 MANNTL model

The error in prediction appears to be proportionate to the scale of the disturbance field being predicted. From Figure 35 the filtered field being predicted varies in the range of 100s of nT and error falls in the 10s of nT. When unfiltered data, varying in the range of 1000s of nT, is predicted as in Figure 36 the error falls to 100s of nT. Although only one model is shown for the sake of brevity, this is the case with all MANNTL experiment 1 models.

Figure 37 shows the results from all models trained on a calibration flight and tested on a later navigation flight. These results do not align with results from the validation set from Section 4.6.2. The model trained with the rectangular TL performed better than either of the cloverleaf models. The only model that performed somewhat consistently to the validation models was the model trained on the rectangular ATL in that the model cannot predict the aircraft disturbance field. The error results in Figure 37, for MANNTL experiment 3, do not match what was actually predicted. The error for the MANNTL experiment 3 was on the 10,000nT scale. This value is not represented in Figure 37 for readability purposes. So far, implementing augmentations that were beneficial for the ATL algorithm are never helpful for any neural network architecture that experimented with.

Figures 38 and 39 show that the MANNTL experiment 2 model can accurately predict the large swings in magnetic intensity and has no large error spikes for the September 17 2D maneuver. However, the MANNTL experiment 4 model has trouble

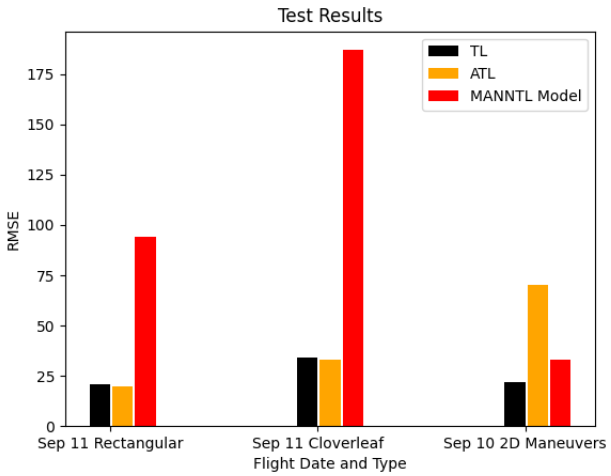

Figure 34: Test results for MANNTL experiment 1.

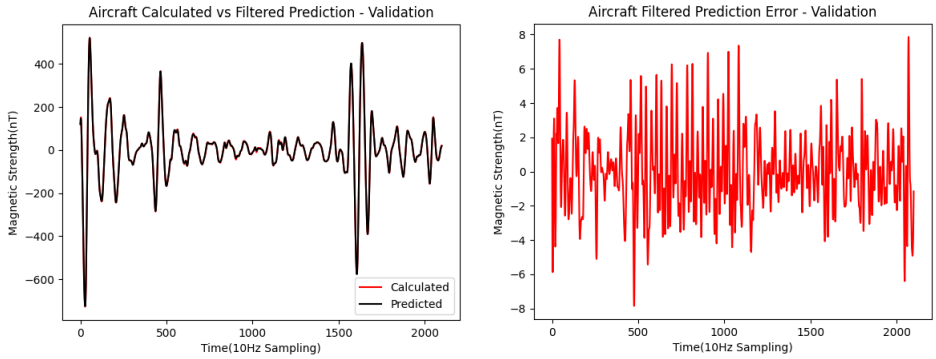

Figure 35: Filtered prediction plots of MANNTL experiment 1, tested on 2D maneuvers from Sep 16. Left: Calculated and filtered aircraft disturbance vs. predicted filtered aircraft disturbance field. Right: Error in filtered aircraft disturbance prediction.

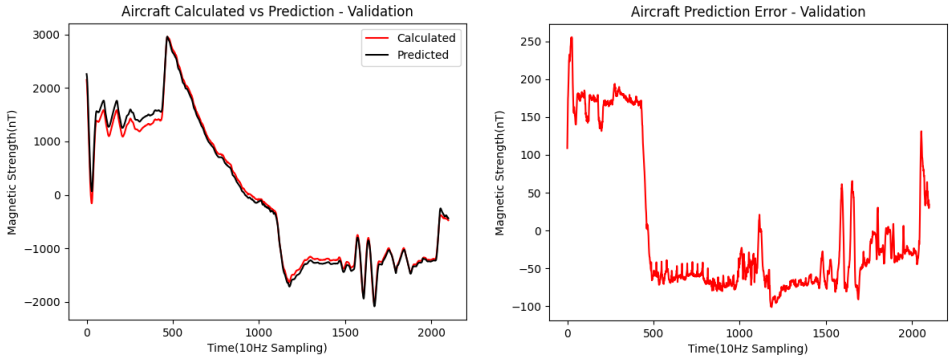

Figure 36: Unfiltered prediction plots of MANNTL experiment 1, tested on 2D maneuvers from Sep 16. Left: Calculated and unfiltered aircraft disturbance vs. predicted unfiltered aircraft disturbance field. Right: Error in unfiltered aircraft disturbance prediction.

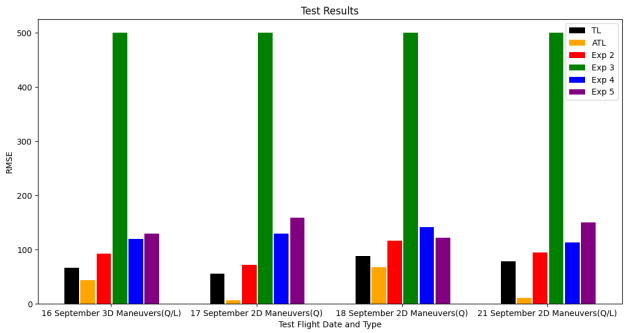

Figure 37: Test results for MANNTL experiments 2-5.

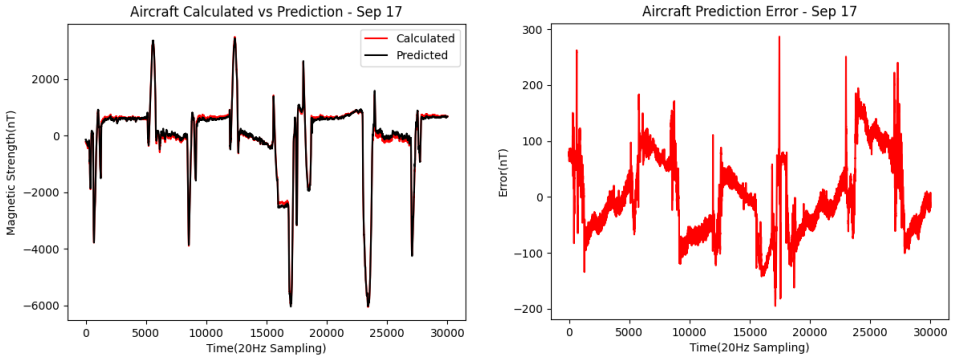

Figure 38: Prediction of unfiltered aircraft disturbance field from MANNTL experiment 2, tested on Sep 17 2D maneuvers. Left: Calculated unfiltered aircraft disturbance field vs. prediction of unfiltered aircraft disturbance field. Right: Error in prediction of aircraft disturbance field.

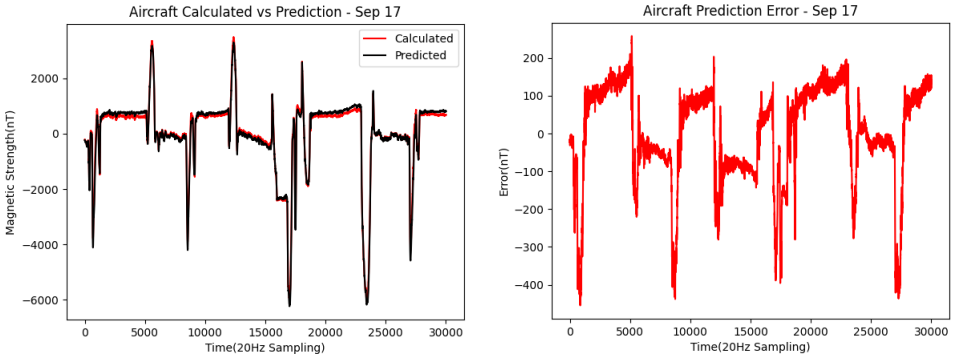

Figure 39: Prediction of unfiltered aircraft disturbance field from MANNTL experiment 4 Left: Calculated unfiltered aircraft disturbance field vs. prediction of unfiltered aircraft disturbance field. Right: Error in prediction of aircraft disturbance field.

predicting the large swings for the same data. This is most likely not the fault of either model architecture. This is most likely an issue caused be the calibration data given to the models. If the model lacks training data that contains these large variations, the model will be ill prepared to predict them as can be seen in Figure 22 from single input experiment 3.

4.8 Results Conclusion

Experiment 3 performed especially poor. I do not believe this was because augmentation data cannot be helpful for ANN models though. Hezel's thesis showed otherwise. The error with experiment 3 resulted in poor augmentation selection. The ATL algorithm was left to choose its own set of beneficial augmentations. That same combination of augmentations were carried over to the neural network model for experiment 3. This might be improved by either handpicking augmentations, such as control surface positioning data. Another method would be to use a tool built for machine learning that can accept the augmentation data and automate the selection of beneficial augmentation combinations much like was used in the ATL algorithm. However, there is a distinct possibility that additional augmentation data does not help at all in a real world scenario such as with the F-16.

It was mentioned in Section 4.6 that regularization was not applied to any of these experiments. It was stated that regularization did not appear to help in early models. However, in Figures 21 and 23 the effects of overfitting vs. generalization can be seen. Single input experiment 2 displayed the model almost memorizing the training data at the expense of generalizing. Single input experiment 4 performed objectively worse on training data but still performed better in validation. Maybe if regularization was added to single input experiment 2, it could have performed better.

The MANNTL model performed poorly at all stages. This result was somewhat

expected with this paper representing its first iteration. There are currently many points of failure to consider in the MANNTL model. The first is data normalization. Currently, both inputs are normalized by the same scale. Separately scaling the two inputs, or changing which scale the two are normalized by could make a big difference. However, the problem could lie with how the dot product is applied to the X vector outputted by the ANN trained on unfiltered data. For example, in experiment 3, both the filtered and unfiltered inputs shared the same set of augmentation data. This is not strictly necessary though. Training on unfiltered data with many augmentations that funnels down to an X vector of size 18 in order to perform the dot operation on the filtered data using only the 18 TL equations could be successful. A final solution could be to switch the positions of the filtered and unfiltered inputs while training. Training the ANN within the MANNTL model on filtered data could yield an X vector output closer to what the TL algorithm would output.

V. Conclusions

There is much to be improved upon considering the results of both ANN models presented in this thesis. There were multiple experiments that displayed the shortcomings of my experimental design and the MANNTL model. Concurrent research is being performed on MagNav by Daniel Clarke to determine what accuracy of aircraft disturbance field prediction is needed in order to reliably navigate. It is expected that sub 10nT will be needed in order to navigate reliably using solely MagNav. This level of accuracy was unfortunately not seen in any of the performed experiments.

5.1 Future Work

5.1.1 General Neural Network Improvements

As mentioned in the previous Chapter, it was shown that the selected augmentations used in all ANN models were detrimental. But this could be attributed to bad selections of augmentation data. Opting for a more *handpicked* method of selection or even using a machine learning add-on tool that can determine the best augmentations could yield better, and more consistent results for both model architectures.

Regularization also deserves to be revisited. Regularization was written off in early experiments but some results from experiments showed that it may have a more positive effect than initially seen.

As for the MANNTL model, there is much more optimization to be done. In its current state, it could possibly beat TL and ATL should it simply be made deeper. However, ANN cannot just be made deeper indefinitely. Special techniques and tools, such as residual network connections, are needed in order for the models weights to remain stable and still be able to describe the data given to model. More improvements could possibly be made to the normalization of the data, how the input data

is inputted, and the size of the output layer of the ANN.

Bibliography

1. UAV Navigation in depth: Magnetometers, why are they critical for UAV navigation?, 8 2018.

2. Aaron Canciani and John Raquet. Absolute Positioning Using the Earth's Magnetic Anomaly Field. *Navigation, Journal of the Institute of Navigation*, 63(2), 2016.

3. British Geological Survey. The Earth's Magnetic Field: An Overview.

4. Micheal A. Nielsen. *Neural Networks and Deep Learning*. Determination Press, 2015.

5. Aravind Pai. https://blogs.nvidia.com/blog/2018/08/02/supervised-unsupervised-learning/. 2 2020.

6. 7 Types of Neural Network Activation Functions: How to Choose?

7. François Chollet. *Deep Learning with Phyton*. 2018.

8. Chandra C. Chatterjee. Basics of the Classic CNN, 7 2019.

9. National PNT Advisory. Board comments on jamming the global positioning system - a national security threat : Recent events and potential cures. *New York*, 2010.

10. Jie Jiang, Xiao Li, Guangjun Zhang, and Xinguo Wei. Fast star tracking technology in star sensor. *Beijing Hangkong Hangtian Daxue Xuebao/Journal of Beijing University of Aeronautics and Astronautics*, 32(8), 2006.

11. James S. McCabe and Kyle J. DeMars. Anonymous feature-based terrain relative navigation. *Journal of Guidance, Control, and Dynamics*, 43(3), 2020.

12. William H. Baird. An introduction to inertial navigation. *American Journal of Physics*, 77(9), 2009.

13. Mitchel Hezel. AIR FORCE INSTITUTE OF TECHNOLOGY. Technical report, Air Force Institute, 3 2020.

14. Arnaud Chulliat Patrick Alken Manoj Nair Adam Woods Brian Meyer Michael Paniccia, William Brown Ciarán Beggan Grace Cox Susan Macmillan, W Brown, P Alken, C Beggan, M Nair, G Cox, A Woods, and S Macmillan. The US/UK World Magnetic Model for. pages 2020–2025, 2020.

15. Fiona Armstrong and Wei Teo. Electricity and magnetism, 2020.

16. T. R. Bodger. Examples of two modern, integrated airborne geophysical systems. *US Geological Survey Bulletin*, 1925, 1990.

17. Colin Reeves. Aeromagnetic surveys. Technical report, 2005.

18. William J. Hinze, Ralph R.B. Von Frese, and Afif H. Saad. *Gravity and magnetic exploration: Principles, practices, and applications*. 2010.

19. Qi Han, Zhenjia Dou, Xiaojun Tong, Xiang Peng, and Hong Guo. A Modified Tolles-Lawson Model Robust to the Errors of the Three-Axis Strapdown Magnetometer. *IEEE Geoscience and Remote Sensing Letters*, 14(3):334–338, 3 2017.

20. Isha Salian. SuperVize Me: What's the Difference Between Supervised, Unsupervised, Semi-Supervised and Reinforcement Learning?, 8 2018.

21. The Complete Guide to Artificial Neural Networks: Concepts and Models.

22. CNN vs RNN: Which Neural Network Is Right for You?

23. Jeff Heaton. Ian Goodfellow, Yoshua Bengio, and Aaron Courville: Deep learning. *Genetic Programming and Evolvable Machines*, 19(1-2), 2018.

Acronyms

2DCNN 2 Dimensional Convolutional Neural Network. 29

AFIT Air Force Institute of Technology. 34

AltNav Alternate Navigation. 1, 2, 30

ANN Artificial Neural Network. vi, vii, x, 4, 26, 27, 28, 29, 31, 32, 33, 35, 36, 39, 40, 41, 42, 44, 50, 56, 62, 63, 64, 65

ANT Autonomy and Navigation Technology. 34

ATL Augmented Tolles-Lawson. vi, x, 3, 5, 11, 23, 31, 32, 33, 37, 38, 39, 41, 49, 56, 59, 62, 64

bpf bandpass filtering. 19

CNN Convolutional Neural Network. 26, 27, 28, 29

DL Deep Learning. 25

DRMS Distance Root Mean Square. 2

GLM Global Loss Minimum. 26, 43

GPS Global Positioning System. 1, 32

IGRF International Geomagnetic Reference Field. 7

INS inertial navigation system. 3

LLM Local Loss Minimum. 26, 43

LSTM Long Short-Term Memory. 29

MagEnv Magnetic Environment. 38, 39, 40, 49

MagNav Magnetic Navigation. 2, 3, 6, 30, 64

MANNTL Mixing Artificial Neural Network and Tolles-Lawson. vi, viii, ix, 4, 35, 36, 37, 41, 42, 43, 50, 51, 52, 53, 54, 55, 56, 59, 60, 61, 62, 63, 64

MSL Mean Sea Level. 37, 38, 40

NAMAD North American Magnetic Anomaly Database. 2, 3

nT nano-Tesla. 2, 6, 7, 8, 10, 31, 39, 49, 58, 59, 64

RADAR Radio Detection and Ranging. 39, 49, 50

ReLU Rectified Linear Unit. vii, 25, 28

RL Reinforcement Learning. 24

RMSE Root Mean Squared Error. 31, 42, 57, 58

RNN Recurrent Neural Network. vii, 26, 27, 28, 29

SQ Solar Quiet current. v, vii, 8, 9, 33

TanH Hyperbolic Tangent. vii, 25, 28, 34, 43

TL Tolles-Lawson. vi, x, 3, 4, 5, 11, 12, 16, 17, 18, 21, 23, 31, 32, 33, 34, 35, 37, 38, 39, 41, 42, 50, 59, 63, 64

TPS Test Pilot School. 32, 36, 37

UAV Unmanned Aerial Vehicle. 3, 30, 31

USAF United States Air Force. 32

REPORT DOCUMENTATION PAGE

Form Approved
OMB No. 0704–0188

1. REPORT DATE *(DD–MM–YYYY)*	2. REPORT TYPE	3. DATES COVERED *(From — To)*
25–03–2021	Master's Thesis	Sept 2019 — Mar 2021

4. TITLE AND SUBTITLE

Modelling Aircraft Disturbance Fields for Magnetic Navigation Using Dense ANNs and the Novel MANNTL Architecture

5a. CONTRACT NUMBER

5b. GRANT NUMBER

5c. PROGRAM ELEMENT NUMBER

6. AUTHOR(S)

Kyle A. Emery

5d. PROJECT NUMBER

5e. TASK NUMBER

5f. WORK UNIT NUMBER

7. PERFORMING ORGANIZATION NAME(S) AND ADDRESS(ES)

Air Force Institute of Technology
Graduate School of Engineering and Management (AFIT/EN)
2950 Hobson Way
WPAFB OH 45433-7765

8. PERFORMING ORGANIZATION REPORT NUMBER

AFIT-ENG-MS-21-M-034

9. SPONSORING / MONITORING AGENCY NAME(S) AND ADDRESS(ES)

Office of Naval Research
875 North Randolph Street Suite 1425
Arlington, VA 22203
DSN: (703)696-4214
Email: Richard.t.willis@navy.mil

10. SPONSOR/MONITOR'S ACRONYM(S)

ONR

11. SPONSOR/MONITOR'S REPORT NUMBER(S)

12. DISTRIBUTION / AVAILABILITY STATEMENT

DISTRIBUTION STATEMENT A:
APPROVED FOR PUBLIC RELEASE; DISTRIBUTION UNLIMITED.

13. SUPPLEMENTARY NOTES

14. ABSTRACT

The ability to use GPS for navigation is becoming increasingly limited in certain areas of the world. Knowing this, the Air Force Research Labs is constantly looking for ways to improve alternate navigation methods such as magnetic navigation. In the interest of making advancements in aircraft disturbance field modelling, Lieutenant Emery recreates models from previous works to prove results. Lieutenant Emery also introduces a novel model architecture that attempts to mix the filtering properties of Tolles-Lawson with the non-linear capabilities of an artificial neural network. The introduction of this model could present better aircraft disturbance field modelling and in turn, more reliable magnetic navigation in regions where GPS is not available.

15. SUBJECT TERMS

16. SECURITY CLASSIFICATION OF:			17. LIMITATION OF ABSTRACT	18. NUMBER OF PAGES	19a. NAME OF RESPONSIBLE PERSON
a. REPORT	b. ABSTRACT	c. THIS PAGE			Major Joseph A. Curro, AFIT/ENG
U	U	U	UU	70	19b. TELEPHONE NUMBER *(include area code)* (312)785-3636x4620, joseph.curro@afit.edu